Materials for Rechargeable Lithium-Ion Batteries

Cary M. Hayner, Xin Zhao, and Harold H. Kung

Department of Chemical and Biological Engineering, Northwestern University, Evanston, Illinois 60208-3120; email: hkung@northwestern.edu

Annu. Rev. Chem. Biomol. Eng. 2012. 3:445–71

First published online as a Review in Advance on April 17, 2012

The *Annual Review of Chemical and Biomolecular Engineering* is online at chembioeng.annualreviews.org

This article's doi:
10.1146/annurev-chembioeng-062011-081024

1947-5438/12/0715-0445$20.00

Keywords

anode material, cathode material, electrolyte, Li-ion battery

Abstract

The lithium-ion battery is the most promising battery candidate to power battery-electric vehicles. For these vehicles to be competitive with those powered by conventional internal combustion engines, significant improvements in battery performance are needed, especially in the energy density and power delivery capabilities. Recent discoveries and advances in the development of electrode materials to improve battery performance are summarized. Promising substitutes for graphite as the anode material include silicon, tin, germanium, their alloys, and various metal oxides that have much higher theoretical storage capacities and operate at slightly higher and safer potentials. Designs that attempt to accommodate strain owing to volumetric changes upon lithiation and delithiation are presented. All known cathode materials have storage capacities inferior to those of anode materials. In addition to variations on known transition metal oxides and phosphates, other potential materials, such as metal fluorides, are discussed as well as the effects of particle size and electrode architecture. New electrolyte systems and additives as well as their effects on battery performance, especially with regard to safety, are described.

INTRODUCTION

Rechargeable batteries of different chemistries have been developed over the years, and they have been commercialized for various applications according to their properties. However, rechargeable batteries have not yet replaced primary (nonrechargeable) batteries as the dominant energy storage device in general because of their high cost for a limited cycling life, unsatisfactory energy density, low power capability, and, in particular, slow recharging. The recent rapid proliferation of handheld electronic and communication devices, such as smart phones, tablets, and laptop computers, has increased the demand for rechargeable batteries sharply. Along with this expanding market comes an increasing demand for improved battery performance: lighter weight, longer cycling life, faster recharging, and lower cost. In the past decade, the lithium-ion (Li-ion) battery has emerged as the most desirable device to meet these demands. It has the highest energy and power density among rechargeable batteries (**Figure 1**) (1) and relatively long cycling life.

At the same time as the market for rechargeable batteries is expanding with portable electronics, the emerging market for plug-in hybrid and battery electric vehicles is poised to take off, and it could dwarf the portable electronics market. These vehicles are more environmentally friendly than conventional vehicles powered by internal combustion engines, and their cost of operation depends much less on the uncertain price of crude oil. However, for this vehicle market to be realized and for electric-drive vehicles to become the preferred mode of personal transportation, the cost and performance of these vehicles need to rival those of conventional vehicles (2, 3).

Important measures of the performance of an electric-drive vehicle related to its battery include range (how far the vehicle can go between battery charges), power (maximum and acceleration speed), safety (consequence of battery rupture, especially in a crash), convenience (charging time, passenger and trunk space), cost of ownership, and reliability. The battery, as the heart of the propulsion system, plays a critical role in all of these characteristics, which are dictated by the

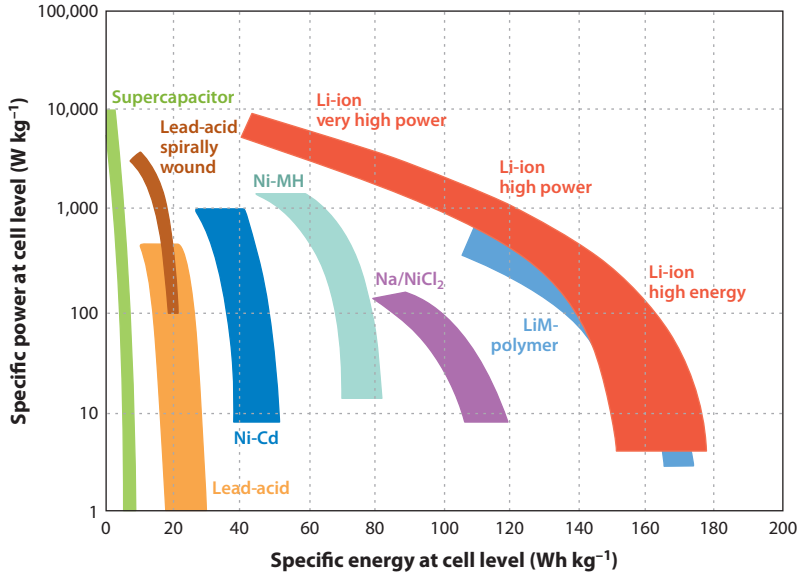

Figure 1

A comparison of the energy and power densities of common rechargeable batteries. Li-ion batteries are superior to the others. Figure adapted from Reference 1. Abbreviation: MH, metal hydride.

material properties of the battery components as well as their fabrication, packaging, and layout. This review provides a broad overview of and describes recent important developments in three major components of Li-ion batteries: the anode, the cathode, and the electrolyte system. Some novel nanomaterial systems applied to Li-ion batteries are presented; how the material morphology, architecture, and properties can be tailored to enhance the performance of Li-ion batteries is emphasized.

BATTERY REQUIREMENTS

The driving range has been cited as a major hurdle for widespread acceptance of electric-drive vehicles. To understand what is necessary to overcome this, it is helpful to estimate the amount of electrical energy a battery must store to provide a driving range comparable with that of a conventional vehicle. Currently, approximately 20% of the energy in the gasoline injected into an internal combustion engine of a standard automobile is consumed in city driving, which includes moving the automobile and operating the accessories (4). A typical full-size automobile, such as a 2011 Chevrolet Malibu or Ford Fusion, carries 17 gal of gasoline and has an average 380-mile range for city driving (22.3 mpg). Using the National Institute of Standards and Technology standard for the energy equivalent of gasoline [1 US gal = 33.41 kWh (114,000 Btu)], the typical vehicle would carry 568 kWh energy in a tank of gasoline, and the propulsion system would deliver 114 kWh (20%) for city driving, which corresponds to 300 Wh mile^{-1}. This is the gross energy consumption to operate a conventional vehicle. Regenerative braking would decrease the energy need by up to 5%, reducing the net energy demand to 285 Wh mile^{-1}. Using a different approach and incorporating future high-efficiency vehicle technologies, Wagner and coworkers (3) estimated a more optimistic net energy demand of 178 Wh mile^{-1}. For illustrative purposes, in the following discussion we will use a somewhat conservative value of 250 Wh mile^{-1}, which is equivalent to 95 kWh delivered energy for a 380-mile range.

The energy output from a battery and the energy delivered for propulsion are related by the efficiency of the electric motor. Fortunately, the energy conversion efficiency of an electric motor is high, >90% (5). Thus, assuming a 90% efficient motor, the onboard battery of a standard vehicle would need to be capable of delivering 106 kWh (= 95/0.9 kWh). Typically, the operation window of a battery is a fraction (approximately 70%) of its fully charged and discharged capacity to avoid the life-shortening deep charge/discharge. Thus, the storage capacity of the battery would need to be 151 kWh.

A more system-level comparison between electric-powered and conventional vehicles in terms of energy consumption would start with the electrical energy from the grid needed to charge the battery to equip the vehicle for a 380-mile driving range. For the conventional vehicle, the corresponding starting point would be gasoline delivered from the gas pump. An even higher-level system comparison would start with the fossil fuel for the conventional vehicle and the energy source that generates the grid electricity. For the discussion here, we start with grid power. For batteries, the difference in the amount of energy downloaded from the grid during charging and delivered during discharge for operation can be substantial. The difference depends on the charge/discharge rate and can be represented by the hysteresis in the voltage versus state of charge curves, as shown schematically in **Figure 2**. In the charged state of a Li-ion battery, Li is concentrated at the anode and depleted at the cathode. The standard electrochemical potentials of Li in this pair of electrodes would determine the open circuit voltage, which is a thermodynamic value. When discharged from a fully charged state, the battery starts at a high voltage, as shown in **Figure 2**. As charge is depleted, the voltage drops. On average, however, the voltage output is lower than the open circuit voltage because of ohmic losses and overpotential owing to rate processes

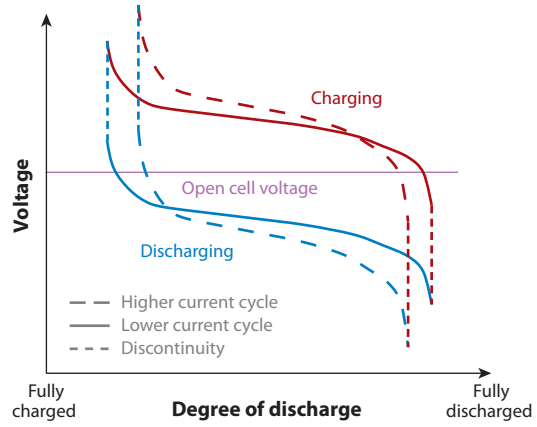

Figure 2

Illustrative voltage curves as a function of state of charge of a battery for charging and discharging cycles at constant current. Dashed lines indicate a higher current cycle and solid lines a lower current cycle. Generally, the voltage is lower than the open cell voltage during discharge and higher during charging because of losses related to various rate processes. The difference between the charging (energy input) and discharging (energy output) branches is larger at higher currents, which indicates the lower efficiency of energy storage.

associated with the chemical reactions and diffusion of Li extracted from the anode material and incorporated into the cathode material. At the end of the discharge, the battery is recharged by an external power source such as the power grid. The average voltage needed to charge the battery is always higher than the open circuit voltage, again owing to losses associated with various rate processes. A more common method of recharging a battery is constant voltage (line voltage after a transformer) instead of constant current. The general shape of the charge/discharge curves is similar to those shown in **Figure 2**, although the details differ. For the Li-ion batteries used currently in handheld electronics, this cycling loss is approximately 30% for a typical operation. Thus, an electric vehicle would consume 151 kWh of grid electricity to deliver 106 kWh for driving 380 miles, with the energy stored in a 151 kWh battery.

Ideally, the entire electric-drive system should be no heavier and occupy no more space than an internal combustion engine propulsion system plus the gasoline. For illustrative purposes, we use 230 kg (507 lb) as the desired weight of a battery pack; this is roughly the weight of an engine block. In the current battery design, typically only 20–25% of the weight of the pack is due to the electrochemically active materials in both electrodes. The rest is from the binder, separator, electrolyte, current collector, housing, and associated protective and control electronics and insulation. Reducing the weight of these other components would reduce the specific energy density requirement of the active components accordingly, as illustrated in **Figure 3*a***. Thus, in a current battery that has only 20% by weight of active components, the energy density of these active components needs to be approximately 2.5 Wh g^{-1}. If the weight fraction of the active components is increased from 20% to 40%, the required energy density of the active components can be reduced to 1.2 Wh g^{-1}.

In a battery, energy is exchanged with the surroundings when electrons are transferred between the two electrodes across a potential gradient. The relationship among the energy density of the electrodes, E, the average voltage across the electrodes, V_{ave}, and the specific charge capacities of the anode, C_A, and the cathode, C_C, can be expressed by the relationship:

$$E = V_{ave}/(1/C_A + 1/C_C). \quad 1.$$

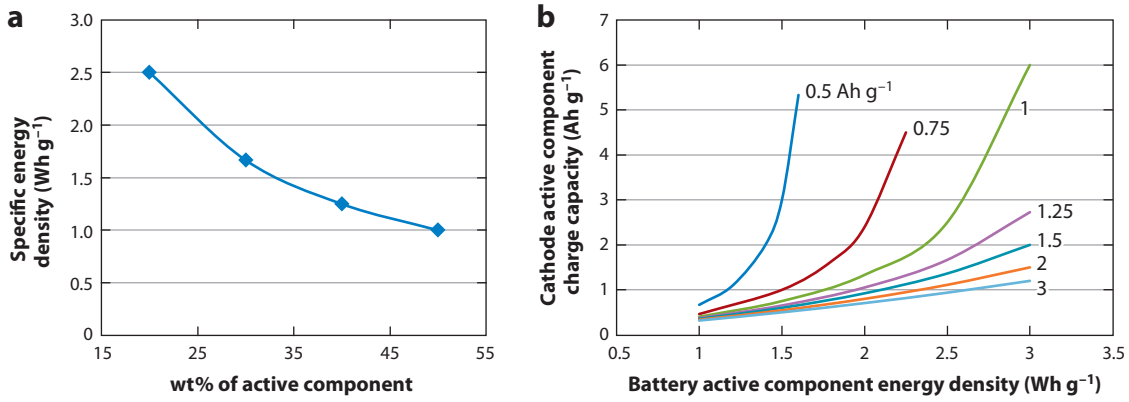

Figure 3

(*a*) Dependence of the specific energy density of active components on their weight fraction in a 230-kg battery pack that has a maximum capacity of 151 kWh but 106 kWh usable capacity. (*b*) Specific charge storage capacity of a cathode material when paired with anode materials of different charge storage capacities, as a function of the active component energy storage capacity for a 3.5-V battery.

Figure 3*b* shows the relationship between the charge storage capacities of the anode and cathode materials and the battery energy capacity, according to Equation 1, for various C_A. From the equation, an electrode material is utilized the most efficiently when C_A and C_C are identical. The current generation of Li-ion batteries employs as the active anode material graphite, which has a theoretical charge storage capacity of 0.384 Ah g^{-1}. A cathode material of 1.1 Ah g^{-1} would be needed to form a 1-Wh g^{-1}, 3.5-V Li-ion battery, which is beyond any known metal oxide cathode material. Therefore, the current battery components cannot meet the target requirements for an electric vehicle.

For anode materials such as graphite and silicon, the theoretical C_A values are 372 and 3,579 mAh g^{-1}, respectively, and for a $LiCoO_2$ cathode, C_C is 135 mAh g^{-1}. **Figure 3*b*** shows that large improvements in total cell capacity can occur with an increase in anode specific capacity up to ~1.25 Ah g^{-1}. Anode electrodes based on Si can possess storage capacities >3.5 Ah g^{-1}. If a cathode material of a storage capacity of ~0.8 Ah g^{-1} could be found, batteries could be built to satisfy the range requirement, and electric-drive transportation systems would be competitive with conventional vehicles if the power, cost, and safety requirements could be met also.

LITHIUM-ION BATTERY BASICS

A typical battery converts chemical energy into electrical energy through a controlled thermodynamically favorable chemical reaction. For a rechargeable battery, this transformation must be reversible. This overall reaction is partitioned into two half-reactions, each of which involves reaction with or removal of Li or Li ions from the active material. By convention, reduction (gain of electrons and Li ions) occurs at the cathode, whereas oxidation (loss of electrons and Li ions) occurs at the anode during a discharge reaction, i.e., when the battery delivers energy. To control the rate of electron transfer, the cathode must be physically and electrically isolated from the anode using an ionically conductive but electrically insulating medium, typically a liquid or polymeric electrolyte. Often a porous, electrically insulating separator is used for mechanical separation between the two electrodes to prevent short circuit (*6*).

The overall chemical reaction employed in the current generation of Li-ion batteries is:

$$0.5\mathrm{Li} + \mathrm{Li}_{0.5}\mathrm{Co}_2\mathrm{O}_4 \leftrightarrow \mathrm{LiCoO}_2.$$

In the fully charged state, Li is stored in the anode material (e.g., graphite). During discharge, Li migrates from the anode through the electrolyte to the cathode in the form of Li^+ ions and inserts into the cathode (e.g., $Li_{1.5}Co_2O_4$). Simultaneously, electrons are removed from the anode (oxidation); are transferred through an external circuit, which creates current to power a load; and enter the cathode (reduction). The discharge process continues until the potential difference between the two electrodes becomes too low, at which point the cell is fully discharged. This process is reversed during charging.

During the initial cycle of a battery, a thin film, known as the solid electrolyte interphase (SEI), spontaneously forms on the surface of electrodes owing to the decomposition of electrolyte. This film is usually electrically insulating but ionically conductive. Formation of the layer occurs predominantly at the graphitic anode, which operates at potentials at which the electrolyte is thermodynamically unstable (less than 600 mV versus Li/Li^+), and creates a complex heterogeneous collection of phases and layers having many secondary interfaces. The composition, behavior, and properties of the SEI vary with different electrode/electrolyte systems and operating conditions, and it is currently the focus of numerous studies on interfacial structure and electrochemical dynamics. In conventional graphitic anodes, SEI growth occurs only during the first charge/discharge cycle to yield a stable passivating layer. However, in next-generation intermetallic anode systems, the SEI morphology changes at different potentials, which indicates a dynamic process (7). This dynamic growth has been used to explain the storage capacity loss observed in many intermetallic anode systems. The SEI of a stable electrode system must act as a passivating protective layer that does not interrupt Li diffusion or reversible Li insertion reactions over repeated charge/discharge cycles.

ANODE MATERIALS

Since the launch of a commercial Li-ion battery by Sony in 1991, graphite has been the predominant anode material. Graphite is a crystalline, layered material consisting of individual sp^2-bonded graphene sheets held together by van der Waals forces. It was selected as the anode material because it is inexpensive, easy to handle, and abundant as well as has good cycling stability and safety features (8). Because Li interacts weakly with graphite, its intercalation into graphite occurs at approximately 100 mV, which is sufficient to prevent plating of Li and formation of Li dendrites that could short the electrodes and cause thermal instability (9), while maintaining a relatively high energy density of the cell. When used as the anode in Li-ion batteries, graphite has a theoretical capacity of 372 mAh g^{-1} (gravimetric basis) and 830 Ah L^{-1} (volumetric basis).

Graphite intercalates lithium reversibly to form LiC_6, according to the following reaction:

$$\mathrm{C}_6 + \mathrm{Li}^+ + \mathrm{e}^- \leftrightarrow \mathrm{LiC}_6.$$

The diffusion of Li into (charge/intercalation) and out of (discharge/deintercalation) graphite causes volumetric changes of up to ~10% because Li ions occupy space between graphene layers, slightly expanding the structure (10).

During the past decade, much research effort has been directed toward identifying alternative anode materials that involve new chemistry and are capable of higher theoretical capacity, higher charge/discharge rate, and greater electrode stability. Candidates for next-generation anode materials include insertion alloys (Si, Sn, Ge), redox metal oxides, and carbon allotropes (graphene, carbon nanotubes).

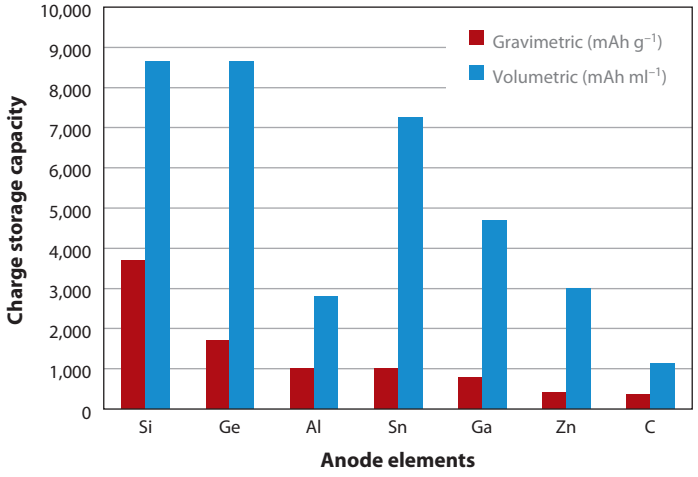

Figure 4

Theoretical gravimetric and volumetric capacities for selected anode elements. Adapted from Reference 14. Copyright © 2007 Royal Society of Chemistry.

In general, insertion alloys provide the highest volumetric and gravimetric energy density for Li-ion batteries. For this reason, they are among the most appealing and competitive materials for new generations of anodes. Indeed, electrochemical alloying of Li with many metals has been studied since the 1970s (11). However, as a trade-off for the enhanced charge storage, these alloy materials experience extreme unavoidable expansion and contraction as Li ions enter and exit the structure, respectively. These volumetric changes lead to rapid deterioration of the morphology of the active material (cracks, particle isolation, pulverization, etc.) that limits the practical lifetime of these electrodes to a few charge-discharge cycles (12, 13). Much research has been performed to improve alloy cycling stability, which is discussed below. **Figure 4** shows the theoretical gravimetric and volumetric capacity values for several potential anode elements (14).

Silicon, which is cheap and abundant and possesses the highest energy density known [~3,579 mAh g^{-1} for $Li_{3.75}Si$ (15)], has been the focus of many investigations. The electrochemical lithiation of silicon was first studied in the late 1970s to investigate the use of silicon to replace lithium metal as the negative electrode in the high-temperature Li/FeS_2 system. Since then, the equilibrium phases have been determined to be $Li_{12}Si_7$ ($Li_{1.71}Si$), Li_7Si_3 ($Li_{2.33}Si$), $Li_{13}Si_4$ ($Li_{3.25}Si$), and $Li_{21}Si_5$ ($Li_{4.2}Si$) (16, 17). The most lithium-rich structure ($Li_{4.2}Si$) gives a specific capacity of ~4,200 mAh g^{-1} on the basis of the weight of Si. However, when silicon is electrochemically lithiated at room temperature, the $Li_{4.2}Si$ phase is not observed; instead, a metastable $Li_{15}Si_4$ ($Li_{3.75}Si$) phase is observed, which corresponds to a theoretical capacity of 3,579 mAh g^{-1}. Upon initial lithiation, the crystalline Si structure undergoes electrochemically driven solid-state amorphization, in which the Si structure loses its crystallinity to become an amorphous Li_xSi alloy (18–21). This irreversible amorphization occurs during the initial lithiation as a single plateau at approximately 100 mV versus Li/Li^+, and it prevents any of the crystalline equilibrium compounds from forming. Subsequent lithiation of the amorphous silicon occurs with two plateaus (~300 and 100 mV) (22), which suggests the formation of two distinct amorphous lithium silicides (Li_xSi and Li_ySi) with different local environments and short-range orders. Because this irreversible amorphization prevents any of the crystalline equilibrium compounds from forming, probing structural changes is difficult, as many traditional spectroscopic techniques are applicable only to crystalline compounds. Solid-state NMR (23) and pair distribution function analysis (24) are two techniques

that have provided useful insight into the local environments of these amorphous materials. From transmission electron microscopy studies, it is known that Si is lithiated via a core-shell process (25) owing to the surplus of Li ions from the electrolyte and slow solid-state diffusion through the active material. Additionally, scanning electron microscopy studies on patterned single-crystal Si wafers demonstrate that the initial lithium insertion is anisotropic; lithiation along the <110> direction is the most facile (26). After the initial cycling, however, the active materials become amorphous and subsequently undergo isotropic expansion during lithiation (27).

To accommodate up to 3.75 Li atoms per silicon atom, the silicon structure also undergoes a tremendous lattice expansion upon lithiation: more than 250% volume expansion. This results in cracking and disintegration of the electrode, which lead to active material loss via reduced electronic contact with the electrode and severe capacity loss. One approach to mitigate the pulverization of the Si structure is to move to nanostructured materials that can better accommodate the strain. Various approaches have been investigated along this direction. One example is to disperse Si nanoparticles between aligned graphene sheets to form a Si/graphene composite (28). Flexible graphene sheets accommodate the large volume variations during cycling and prevent particle aggregation or isolation, which results in significantly enhanced cycling stability. Other approaches include reducing the Si particle size (29), using thin films (30–32) or nanowires (25), dispersing into an inactive/active matrix (33–36), preparing 3D porous structures (36–38), mixing/coating with carbon (39–43), and optimizing polymer binders (44, 45). Some engineered structures, such as chemical vapor deposition (CVD)-grown nanowires and amorphous thin films, have shown promising capacity stability, but they do not offer a high enough density of active material in the electrode for a viable battery and still fail when electrode thickness increases (46).

Tin, similar to Si, is able to bind up to 4.2 Li ions per host atom. However, owing to its increased atomic mass, the maximum specific theoretical capacity of Sn is 960 mAh g^{-1}. Similarly, germanium is capable of storing 1,600 mAh g^{-1} capacity by transforming into $Li_{4.4}Ge$. Both of these materials have been the focus of many studies. Sn has been studied in metallic form as well as in Sn-based composite oxides (47) and alloys with other active (such as Sb) (48) or inactive (such as Cu) metals. These intermetallic compounds help reduce the effects of structural changes and displacement reactions on reversibility by diluting the Li content. In the case of a Cu-Sn alloy, for example, Cu acts as an inactive matrix to buffer volume variations when Sn is displaced upon lithiation to form the alloy Li_xSn. Structural similarity of the intermetallic compound before and after lithiation, such as in the Cu_6Sn_5 to Li_2CuSn transition, can also contribute to cycling stability (49). However, the theoretical capacity of Cu_6Sn_5, 584 mAh g^{-1}, is much lower than that of other anode materials such as Si and Ge. To increase the total capacity, one approach is to use composite Cu_6Sn_5-Sn electrodes, wherein the Cu-Sn matrix stabilizes the Sn particles. Indeed, this method has proven successful for increasing electrode capacity while maintaining cycling stability for many cycles (50).

Transition metal oxides form another class of anode materials, and titanates are one of the most studied. One of the greatest advantages of titanate anodes is that Li intercalates within the stability window of carbonate electrolytes, thus avoiding the reductive decomposition of the electrolyte solvents. For example, $Li_4Ti_5O_{12}$ (LTO) intercalates Li at 1.6 V versus Li^+/Li, which minimizes any side reactions and avoids the formation of SEI, thus leading to improved reliability and calendar life:

$$Li_4Ti_5O_{12} + 3Li^+ + 3e^- \rightarrow Li_7Ti_5O_{12}.$$

The surface of LTO thus remains fresh for Li transport, and in particular, full use can be made of a large specific surface area to enhance the capacity and rate capability within LTO nanostructures.

Another advantage of LTO is the absence of lattice strain or volume variations, which means that LTO is not susceptible to fracture. This results in a nanostructured LTO anode that is capable of cycling incredibly fast (within a minute or two) and achieving superior cycling stability (51). Unfortunately, the operating voltage of a full cell can be diminished by employing LTO anodes owing to a high Li intercalation voltage. Additionally, the theoretical capacity of LTO is 160 mAh g^{-1}, less than half the theoretical capacity of graphite, which makes it attractive only in applications in which prolonged cycling or excellent safety features are the primary requirements.

Redox metal oxides (MnO_2, NiO, Co_3O_4, Fe_3O_4, Fe_2O_3, etc.) store charges through conversion reactions with Li, within which electrochemical reduction leads to the transfer of at least two Li ions, resulting in nanosized metallic clusters dispersed in a Li_2O matrix (52). Owing to the inherently small size of the clusters, these reactions have shown a favorable reversibility. In general, these materials have higher theoretical capacities than that of graphite. One of the main benefits of conversion reactions is the ability to optimize the cell voltage and capacity. The potential can be tuned by modifying the metal cation (M) employed, as the local structure and strength of the M–O bond directly affects the equilibrium voltage. Furthermore, utilization of low-cost and abundant metals, such as iron and manganese, provides a variety of scalable electrode alternatives. The two major drawbacks with most conversion reaction–based materials are their poor reaction kinetics as well as a large hysteresis in charge/discharge voltages, which is associated with an energetic barrier in the breaking of the M–O bond and the change of electronic conductance.

Carbon allotropes, such as graphene and carbon nanotubes (CNTs), represent another group of attractive electrode candidates for Li-ion batteries. Graphene, a monolayer of sp^2-bonded carbon atoms in a honeycomb crystal lattice (53), can be considered the basic structural element of many forms of carbon. Exploitation of graphene as an anode material and conductive additive for both cathode and anode has occurred since it was first experimentally isolated in 2004 (54) because of its excellent conductivity, chemical stability, and mechanical robustness. Although sometimes debated, it is believed that graphene can achieve a capacity of ~744 mAh g^{-1} theoretically, twice that of graphite. This increase in capacity corresponds to Li ions stored on both sides of isolated graphene sheets (Li_2C_6), as opposed to a single side for the stacked graphitic structure. Furthermore, additional sites such as defects, cavities, and edges of graphene may be able to host extra Li ions. Indeed, graphene anodes with reversible capacities of 540 mAh g^{-1} have been reported (55).

Many graphene-based electrodes are synthesized via graphene oxide precursors that are derived from exfoliation of graphite, a process that typically introduces many defects into graphene. Therefore, unlike graphite, graphene-based anodes exhibit variable Li insertion voltages owing to the nonequilibrium Li insertion sites, which are electrochemically similar to soft carbons. Unfortunately, as a consequence of the inherently high surface area of graphene (2,600 m^2 g^{-1}, theoretical), these anodes suffer from large irreversible capacities owing to extensive formation of SEI during the first cycle.

Single-walled CNTs, similar to graphene, also exhibit twice the Li storage capacity compared with graphite, and they have sloped potential profiles for lithium insertion and removal. The high surface area of CNTs also introduces comparable problems regarding SEI formation and safety issues, which hinder the practical utility of CNT anodes.

ANODE CYCLING STABILITY

The performance of most potential anode materials cannot meet practical requirements owing to inferior cycling stability compared with graphite, and various strategies have been pursued to address this issue. One of the most efficient approaches is to confine the particle size to nanodimensions. In addition to reducing the diffusion length of Li into the core of the particles so that

a higher capacity can be achieved, nanomaterials are able to accommodate Li insertion strain and minimize cracking and disintegration of the electrodes. Specific architectures such as nanotubes and nanowires have proven to be more stable than nanoparticles in many cases. Optimization of the polymer binder also has a significant impact on electrode cycling stability owing to modified adhesion and electrolyte uptake. Common polymer binders include polyvinylidene fluoride and carboxymethylcellulose. Recently, polyacrylic acid (56) and brown algae extract (57) were shown to increase the cycling stability of Si-based anodes.

As mentioned previously, one of the major factors that determine the cycling life of Li-ion batteries is the formation of SEI. Its chemical composition, porosity, thickness, and ionic conductivity are critical to the reliability, rate capability, coulombic efficiency, and life span of an electrochemical cell. One approach to enhance the electrode cyclability is to introduce an electrode additive that reacts more easily than the electrolyte to form a more stable, protective SEI layer on the anode surface. These additives typically decompose at higher voltages (greater than 1 V versus Li/Li^+ for the additive) than the standard electrolyte and therefore form a foundation layer of protection. The particular electrolyte additives used are different for each type of active material but typically involve unsaturated functionalities (carbonyl-, vinyl-, or heterocycle-containing compounds) (58). In choosing electrolytes and additives, the ideal properties include: (*a*) high electronic resistance, (*b*) high transference number, (*c*) high ionic conductivity, (*d*) good adhesion to the active material surface, and (*e*) homogeneous distribution on the surface (59).

A variation of this approach is to encapsulate the nanoparticles during electrode preparation in a conducting shell that is ideally chemically inert, electrically conducting, and porous to Li ion diffusion but structurally flexible to accommodate volumetric variations. Attempts to encapsulate silicon nanoparticles with a graphitized polymer resulted in improved cycling stability but a more graphitized shell, which is electrically more conducting but also mechanically more rigid, which limits its ability to accommodate strains owing to volumetric variations (60).

MAXIMIZATION OF THE RATE CAPABILITY OF ANODES

Because Li ion insertion and removal from an electrode is a rate process, the attainable storage capacity depends on the charge/discharge rates. Therefore, there is significant interest in increasing the rate capability of electrode materials without sacrificing the attainable storage capacity. Various attempts to achieve this include decreasing the dimension of active materials to the nanoscale and developing novel architectures to allow fast Li diffusion.

By decreasing the size of particles from microsize to nanosize, the rate of Li insertion/removal can be improved dramatically owing to shortened Li diffusion pathways within the particles. The characteristic time constant for diffusion is given by $\tau = L^2/D$, where L is the diffusion length and D is the diffusion constant. The high surface area of nanomaterials also provides an increased contact area with the electrolyte and therefore a high Li-ion flux across the interface and rapid Li ion transfer.

A different approach is to engineer electrode architectures to maximize ion and electron transport throughout the electrode and ultimately the rate capability of the battery cell. One example is the creation of a 3D electrode geometry using inverse opals that allows accommodation of a large amount of electrolyte and a short Li diffusion path through active material (61). However, the total active mass of such electrode designs is rather low owing to the excessive mass of the current collector. The use of sacrificial templates to form nanofoams and nanotubes (62) with controllable thickness and diameter is another strategy that has proven successful for increasing rate capabilities. However, this technique is not easily industrially scalable, and the electrodes commonly suffer from low packing densities. A final example is the introduction of nanometer-sized holes into

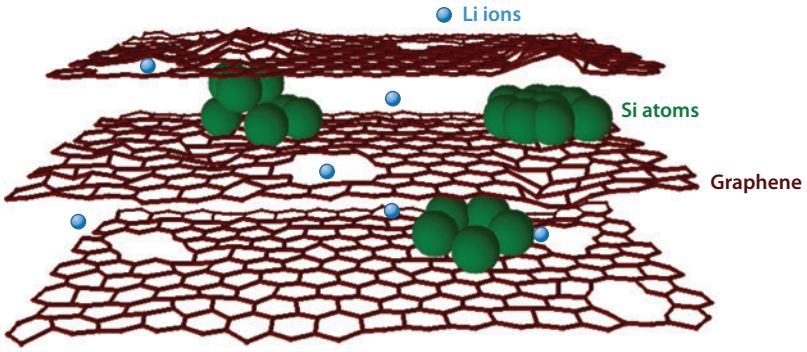

Figure 5

Schematic drawing of a Si-graphenic composite electrode for Li-ion batteries, which is engineered with a flexible, 3D graphenic scaffold derived from graphene sheets with a high density of in-plane, nanometer-sized window-like vacancies that enable rapid cross-plane ion diffusion and hence high rate capacity. Figure adapted from Reference 63. Copyright © 2011 Wiley.

individual layers of graphene in graphene-based electrodes (63). When the graphene sheets are aligned, these holes create randomly positioned cross-plane ion diffusion channels perpendicular to the basal plane that significantly enhance 3D ion mobility through the electrode (**Figure 5**). The main downside of this approach is the cost of the material precursors.

CATHODE MATERIALS

Unlike the anode, for which high–storage capacity materials are known to exist, the comparatively low storage capacity of most known cathode materials has been recognized as a major limiting factor in the overall performance of Li-ion batteries. Since the successful introduction of the $LiCoO_2$ cathode in 1991, other positive electrodes that have been investigated for commercial applications fall mainly into two categories (64, 65). The first group is layered lithium compounds with a close-packed oxygen anion lattice, in which transition metal cations occupy alternate layers between the anions and Li ions are intercalated into the remaining empty layers. The compounds in this group have the advantage of higher operating voltage and specific energy than the second group owing to their highly oxidizing redox-active couples and more compact lattices. These materials are compositional variations of the layered $LiCoO_2$ (**Figure 6*a***), such as $LiNiO_2$, $LiMnO_2$, $LiNi_{1-x}Co_xO_2$, and $LiNi_xMn_xCo_{1-2x}O_2$, as well as 3D spinel structures derived from $LiMn_2O_4$ (**Figure 6*b***), such as the $Li_{1+x}Mn_{2-x}O_4$ system. The second group consists of materials with more open structures, including layered V and Mo oxides such as V_2O_5 and MoO_3, layered or channeled compounds of Mn such as MnO_2, and transition metal phosphates, such as the olivine $LiFePO_4$, with 1D Li ion diffusion channels (**Figure 6*c***). Although they operate at lower voltages, the reduced cost, improved safety, and rate capabilities of these materials compared with the former group make them competitive cathode candidates. In general, oxide systems are preferred over transition metal chalcogenides (sulfides and selenides) because it is difficult to stabilize higher oxidation states of transitional metal ions and achieve cell voltages >2.5 V versus Li/Li^+ in chalcogenides (66–69). For oxide systems, voltages of ≈4.0 V versus Li/Li^+ can be achieved in nonaqueous systems.

The structure of the layered oxides is conducive to rapid Li insertion and extraction. One research emphasis is to replace the costly Co in $LiCoO_2$ with less expensive and less toxic components. Layered Li_xNiO_2 and Li_xMnO_2 ($x \sim 0.55$) were among the materials under intensive

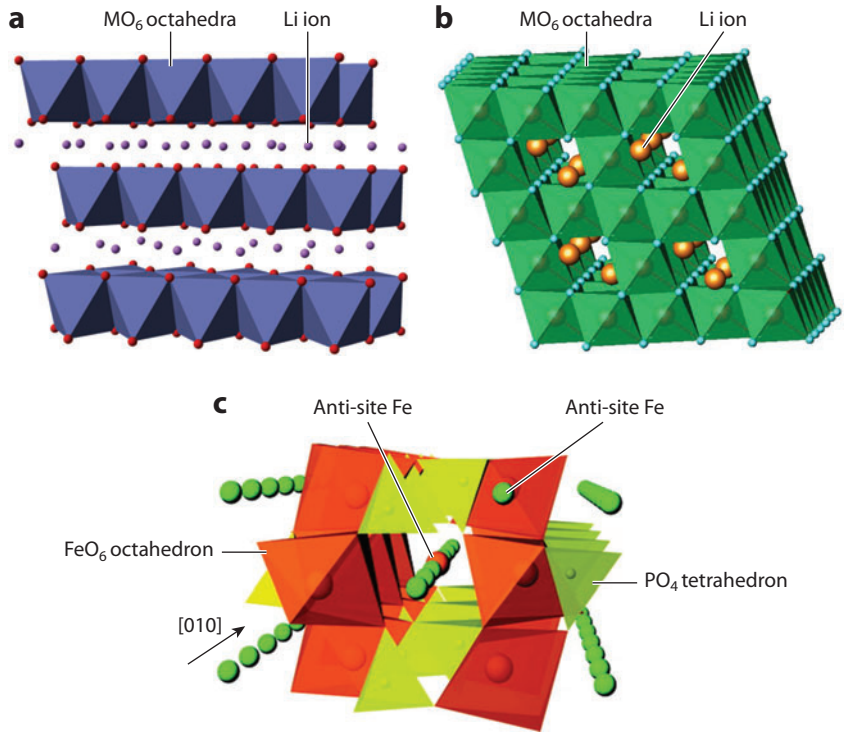

Figure 6

Crystal structures of three typical cathode materials available for commercial Li-ion batteries. Panel *b* taken from **http://www.phy.cmich.edu/people/petkov/nano.html**. Panels *a* and *c* taken from Reference 70. Copyright © 2008 American Chemical Society.

study, but it was soon recognized that Li_xNiO_2 suffers from thermal runaway and is difficult to synthesize, whereas Li_xMnO_2 suffers from a layered to spinel structural transition during cycling that degrades its high-potential (4 V) performance (65, 71, 72). Substitution of Mn by Co or Ni results in diverse layered compositional variations that show improved capacity approaching 200 mAh g^{-1} and experience much slower phase transformation, but the release of oxygen and severe thermal runaway still cause serious safety issues (71–73).

The spinel $Li_xMn_2O_4$, which possesses an edge-shared Mn_2O_4 octahedral framework, demonstrates good structural stability for reversible Li ion insertion/extraction at regular tetrahedral sites in the range $0 < x < 1$ (66, 74, 75). Further insertion of Li ions to $1 < x < 2$ decreases the average valence of Mn ions substantially, leading to a pronounced structural distortion accompanied by capacity degradation due to leaching of Mn ions into the electrolyte. This limits the accessible capacity of $Li_xMn_2O_4$ to 120–125 mAh g^{-1} and a practical operating voltage range greater than 3.5 V (67). Attempts to mitigate these limitations include the creation of highly lithium-rich spinel compositions, such as $Li_{1.06}Mn_{1.94}O_4$ and $Li_{1.12}Mn_{1.88}O_4$, to increase the content of less soluble Mn^{3+}, or introduction of various cation substitutions (Ni, Co, Cr, Ti, Al, etc.) into the spinel lattice to minimize structural alteration, both of which could compromise the theoretical capacity or induce irreversible capacities owing to a change in the energy of the operative redox couple (76–78). Another strategy is to integrate Li_2MnO_3, which is structurally compatible but electrochemically inactive, into the spinel structure (72). The compound $0.3Li_2MnO_3 \cdot 0.7LiMn_{0.5}Ni_{0.5}O_2$ (79) has

been reported to have a reversible capacity up to 300–350 mAh g^{-1} in the voltage window of 2–5 V with profoundly improved rate capability and thermal stability. However, an electrolyte stable at high voltages would be required to match these cathode systems for practical utilization.

Lower voltage redox couples, such as Fe^{2+}/Fe^{3+} in the phosphate olivines $LiMPO_4$ (M = Fe, Mn, Co and Ni), result in lower-voltage electrodes (<2.5 V) and safer battery operation (80–82). They can be used readily with available carbonate electrolytes. The phosphate can be replaced with the polyanion XO_4^{2-} (X = S, Mo, W), and Fe can be substituted by other cations, such as Mn, Co, and Ni. $LiFePO_4$ is being developed into a commercial cathode material. It has a reasonable theoretical capacity of 170 mAh g^{-1} and is structurally stable, environmentally friendly, and cost effective. Nonetheless, its low storage capacity and poor electronic conduction, as well as the presence of inactive Fe^{III} and lithium phosphate impurities in the preparation, limit its potential (81, 83, 84). Other phosphate olivines such as $LiMnPO_4$, $LiCoPO_4$, and $LiNiPO_4$ have higher operating voltages and are under investigation.

NANOSTRUCTURED CATHODES

Similar to anode materials, nanostructured cathode materials have been investigated in attempts to reduce the Li ion diffusion barrier and structural instability as well as to mitigate the intrinsic limitation of ionic conductivity in oxides, so as to achieve higher capacities. For example, conventional $LiCoO_2$ cathodes have a low practical capacity of <140 mAh g^{-1}, far below the theoretical capacity of 273 mAh g^{-1}. However, a capacity of 155 mAh g^{-1} was achieved even at a high rate of 5 A g^{-1} with a hyperbranched $LiCoO_2$ structure composed of ~10-nm-thick branches grown perpendicular to the [001] direction (**Figure 7*a*,*b***) (85). These branched assemblies of $LiCoO_2$ were synthesized by a one-pot fluxing of molten alkali metal salt/hydroxide, which yielded fine control over nanostructures in contrast to conventional solid-state reactions. Another example is $LiFePO_4$. Carbon-coated $LiFePO_4$ nanoplates with a thickness of 30–40 nm along the [010] direction, fabricated by a facile solvothermal method, yielded a high capacity of 165 mAh g^{-1} at 17 mA g and 50 mAh g^{-1} at 5.1 A g^{-1} (86, 87). This is in good agreement with ab-initio calculations and atomistic simulations that showed preferential Li ion transport along the *b*-axis (88, 89). However, a concern with these nanostructures is their chemical instability when exposed to the atmosphere and other interfacial reactions owing to their high surface areas (90).

The equilibrium properties of the cathode material can be affected by reduction of its size, which results in modification of the phase transformation behavior upon Li insertion/extraction. Reduction of the particle size of $LiFePO_4$ and $LiMn_2O_4$ has been shown to change the mechanism of Li ion insertion from a two-phase transformation with a miscibility gap to a single-phase solid-state reaction (92). Mesoporous $Li_{1.12}Mn_{1.88}O_4$ and β-MnO_2 have displayed improved capacity of ~240 mAh g^{-1} with improved cyclability in the voltage range of 2–4.5 V (93, 94), which was ascribed to the relief of strain, and thus a more facile cubic to tetragonal phase transition achieved by the nanometer-thick walls. These highly ordered porous structures were fabricated by impregnation of Mn precursor solution into a silica template. A capacity close to the theoretical value was reported for 8–9-nm-thick $LiMn_2O_4$ nanowires with excellent rate capability (**Figure 7*c*,*d***) (91). A recent study of 15-nm $LiMn_2O_4$ particles suggested disappearance of phase boundaries owing to a shortened Li ion diffusion length and a high surface energy that efficiently stabilized the solid solution state (95). Likewise, $LiFePO_4$ nanoparticles with a size of 40 nm prepared by precipitation exhibited a sloping charge/discharge curve characteristic of pure single-phase behavior (96).

High capacities greater than 300 mAh g^{-1} have been achieved in various nanostructured binary oxides and fluorides. Initial capacities of 650 mAh g^{-1} and 1,240 mAh g^{-1}, which far exceed the theoretical capacity for bulk $Li_xV_2O_5$ ($x < 3$), were obtained in sol-gel processed porous

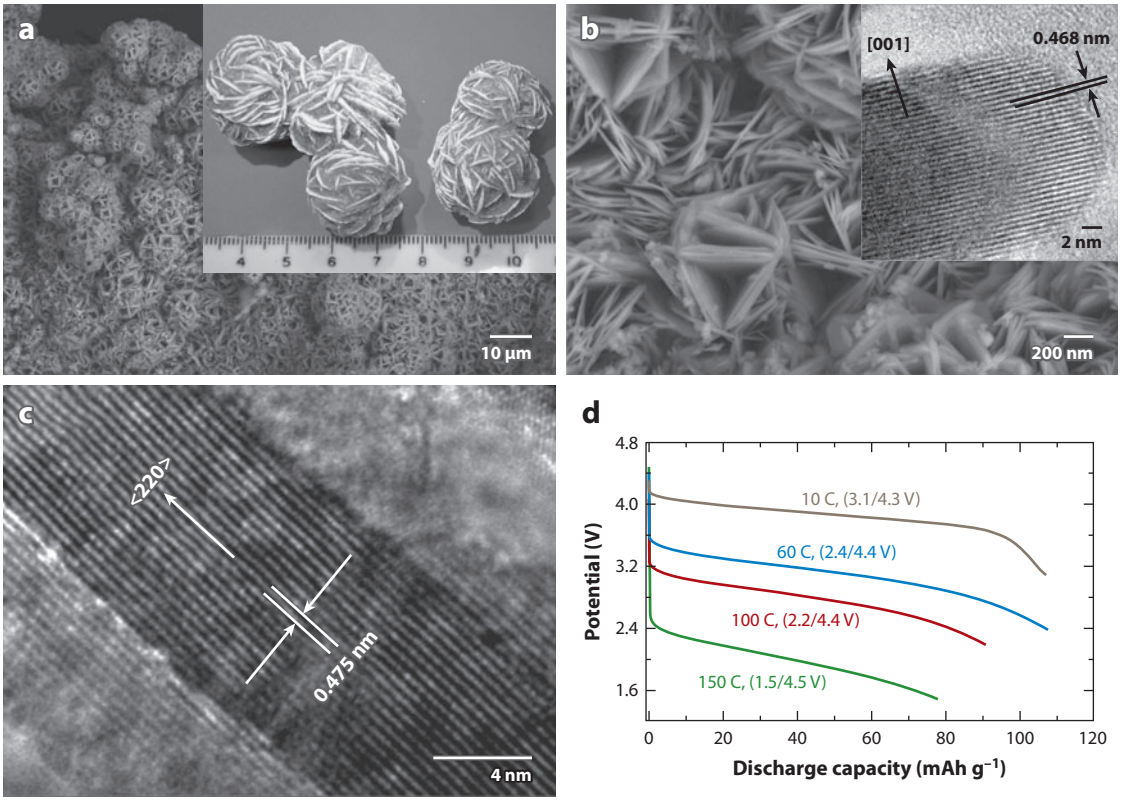

Figure 7

(*a*) Scanning electron microscopy (SEM) image of hyperbranched $LiCoO_2$ nanostructures forming the desert-rose structure shown in the inset (85); copyright © 2008 Wiley. (*b*) High-magnification SEM image of $LiCoO_2$ branches. (*Inset*) Transmission electron microscopy (TEM) image shows the 10-nm-thick branch terminated by rounded faces perpendicular to (001) planes. (*c*) TEM image of an ultrathin $LiMn_2O_4$ nanowire with a diameter of 8–9 nm (91); copyright © 2010 Royal Society of Chemistry. (*d*) Galvanostatic discharge curves of the nanowire in panel *c* at different rates after charging at 1 C (148 mA g^{-1}). Voltage windows are indicated.

V_2O_5 aerogels (97) and vertically grown, nanometer-thick platelets (98), respectively, although these values tended to fade rapidly owing to formation of electrochemically inactive phases and collapse of original architectures upon cycling. Nanoribbons of crystalline V_2O_5 demonstrated increases in the Li diffusion coefficient of several orders of magnitude and completely reversible phase transition into ω-$Li_3V_2O_5$ (99). CVD-grown α-MoO_3 nanorods (100) and prelithiated α-MoO_3 nanobelts fabricated via a hydrothermal approach (101) displayed a reversible capacity of 300 mAh g^{-1} with an improved rate and cycling performance superior to that of their submicrometer-sized counterparts. FeF_3 has a high theoretical capacity of 712 mAh g^{-1} when lithiated to ~1.5 V, and nanostructured FeF_3 undergoes reversible transformation to both LiF and metallic Fe (102, 103). FeF_3 nanocrystallites with a size of 10–20 nm embedded in graphite or carbon black matrices, fabricated through high-energy ball milling, exhibited reversible capacities approaching the theoretical value with respect to the active FeF_3 (104). In comparison, bulk FeF_3 directly mixed with conducting carbon had a low capacity of less than 100 mAh g^{-1} (105), which highlights the importance of particle size reduction and creation of a stable interconnect with the underlying conducting network in FeF_3 composite cathodes.

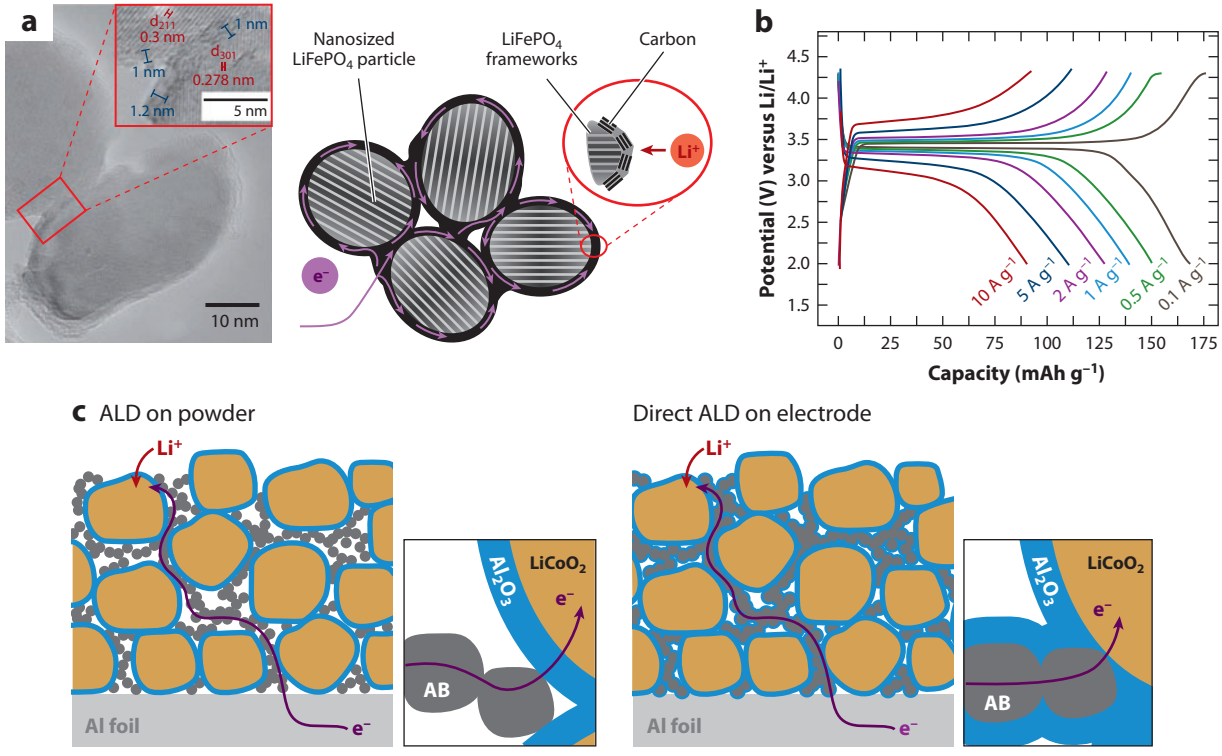

Figure 8

(*a*, *left*) Transmission electron microscopy (TEM) image of 1–2-nm-thick carbon-coated $LiFePO_4$ nanoparticles. (*a*, *right*) A schematic showing their designed structure and complete graphitic carbon coating that facilitated electron transfer (106). (*b*) Galvanostatic charge/discharge curves at different rates in the voltage window of 2.0–4.3 V versus Li/Li^+ (106). Panels *a* and *b* copyright © 2008 Wiley. (*c*) Schematics of transport in $LiCoO_2/Al_2O_3$/acetylene black (AB) electrodes when atomic layer deposition (ALD) is performed first on the powder versus when ALD is performed directly on the composite electrode (116); copyright © 2010 Wiley.

COATING OF CATHODE MATERIALS

Coating has been widely used to facilitate ion transport across the electrode/electrolyte interface and to alleviate side reactions at the interface by forming a stable protective layer. A rich variety of carbonaceous organic compounds such as sucrose (106, 107), glucose (108), block copolymers (109, 110), and ionic liquids (111) have been employed as carbon precursors. An elastic carbon layer can be generated, which may accommodate any Li insertion strain and subsequent volume variations effectively, leading to drastically enhanced capacity retention upon cycling (90). The nature of the carbonaceous coating, including the density and type of functional groups, porosity, and extent of aromatization/graphitization, strongly influences the electrochemical performance of the electrode material (112). Recently, $LiFePO_4$ nanoparticles with a 1–2-nm-thick carbon shell prepared by a solid-state lithiation of $FePO_4$ coated with polyaniline and sucrose attained a discharge capacity of 90 mAh g^{-1} at a current rate of 10 A g^{-1} (60 C) (**Figure 8*a*** and ***b***) (90, 106). A stable capacity of ~50 mAh g^{-1} was reported for nanoporous carbon matrix–encapsulated spherical $LiFeO_4$ nanoparticles fabricated using a combined sol-gel synthesis and solid-state reaction, even at an ultrahigh rate of 230 C (110).

Coating cathode materials with nanometer-thick ceramics is another effective strategy to enhance electrode cycling performance and extend shelf life by preventing direct contact of the active

cores with the electrolyte, decreasing the dissolution of transition metal ions, and suppressing the deleterious phase transition by modifying the Li-site energy and metal ion disproportionation (113). SiO_2, Al_2O_3, MgO, ZrO_2, and metal phosphates have been achieved by methods such as the sol-gel approach, reactive sputtering, and direct assembly of colloidal particles onto cathode materials (2, 113, 114). For example, a 10-nm-thick ZnO-coated $LiNi_{0.5}Mn_{1.5}O_4$ cathode delivered a discharge capacity of ~140 mAh g^{-1} without apparent degradation at elevated temperatures (115). However, control of the coating thickness is critical in maintaining the conductivity owing to the insulating nature of the ceramics. A recent report compared the effect of a conformal Al_2O_3 coating made directly on electrodes by atomic layer deposition (ALD) with a coating on powder samples, which showed that full coverage of the active powder hindered electron transport and thus direct deposition of the coating layer onto electrodes is preferable (**Figure 8*c***) (116). However, realization of conformal nanosized coating on cathode materials without the emergence of secondary phases and aggregation is challenging. Lack of cost-effective and scalable coating processes presents another major barrier for practical implementation of these nanostructures.

DESIGN OF CATHODE MATERIALS

Thermodynamic and computational studies provide useful guidance to the exploration of higher-capacity cathode materials (117, 118). Based on considerations of the number of transferable charges and the oxidation state of the redox-active transition metal, a compound containing a low-valent metal with multiple oxidation states and an anion with a high negative charge-to-mass ratio is preferable for high–specific charge storage capacity. This is illustrated in **Figure 9*a*** for metal phosphates, which shows the limitations of this class of compounds. For energy density, the redox potential needs to be considered as well. Theoretical voltages of delithiated cathode materials at the equilibrium state have been studied extensively. They are determined by the Fermi level of the active redox couple, the inductive effect from the anion, and the lattice structural parameters (68, 117–120). **Figure 9*b*** summarizes some of these results.

Table 1 lists the theoretical voltage averaged over the oxidation state changes, specific capacity, and energy density of some inorganic compounds (117, 121–123). From the specific energy perspective, simple oxides and fluorides as well as olivine silicate polymorphs ($LiMSiO_4$) that possess feasible multielectron reactions and operating voltage compatible with the target window of 3–4.5 V are more favorable (118). Metal fluorides are capable of higher energy delivery than oxides and sulfides, owing to a much stronger electronegativity of fluoride ions and thus a higher operating voltage. The olivine silicate family attains much higher theoretical capacities than do phosphate olivines if the extraction of both Li ions in Li_2MSiO_4 is feasible. However, in terms of practical adoption, kinetics and crystal structural factors must be taken into account. The combined requirements of kinetics, i.e., the mass transport, ion and electron transfer, and reaction reversibility, still call for innovative chemistries and materials engineering.

BEYOND LITHIUM-ION

At present, known systems based on intercalation and conversion chemistry have fundamental limits on specific storage capacities and energy densities. Systems based on different chemistries will be needed to overcome these limitations. One such system is the Li-air battery. Metal-air technologies were explored extensively a decade ago and already have been developed commercially as primary power sources, including zinc-air batteries and fuel cells, both of which are based on aqueous systems. The first nonaqueous Li-air battery was assembled in 1996 by Abraham et al.

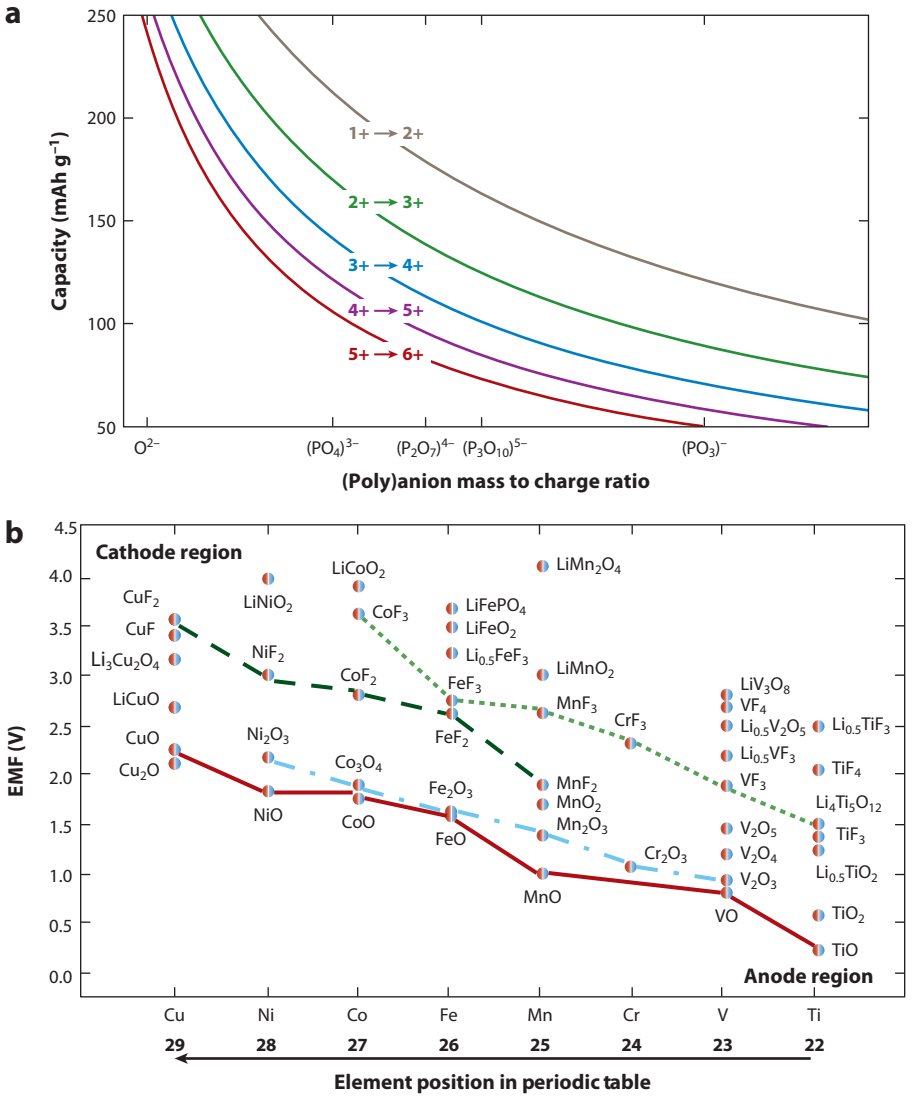

Figure 9

(*a*) Theoretical gravimetric capacity for different redox couples $M^{(n-1)+}/M^{n+}$ as a function of the mass-to-charge ratio of the (poly)anion. Oxides and various phosphate polyanions are indicated on the mass-to-charge ratio axis assuming the mass of iron for the metal element (118); copyright © 2011 American Chemical Society. (*b*) Calculated thermodynamic equilibrium voltage [the so-called electromotive force (EMF), V] of reactions between transition metal compounds and lithium (120); copyright © 2004 Electrochemical Society.

(124, 125), who recognized its rechargeability with the aid of a catalyst, and its applicability for rechargeable cells was demonstrated recently (126–128).

In the discharge cycle of a Li-air battery, O_2 from the environment is reduced by electrons from an external circuit and charge balanced by Li ions from the electrolyte to form the discharge products Li_2O_2/Li_2O. These Li oxides decompose to Li and O_2 upon charging, and the

Table 1 Theoretical average voltage versus Li/Li^+, specific capacity, and specific energy during reactions with lithium for a variety of fluorides, oxides, and lithium compounds (117, 121–123)

Cathode	Voltage (V)	Specific capacity (mAh g^{-1})	Specific energy (Wh kg^{-1})
$LiCoO_2$	3.9	130	507
$LiMn_2O_4$	3.95	148	585
FeF_3	2.74	712	1,951
MnF_3	2.65	719	1,905
CuF_2	3.55	528	1,874
CoF_2	2.86	553	1,578
NiF_2	2.96	554	1,435
CuO	2.25	674	1,517
CoO	1.80	715	1,287
NiO	1.81	718	1,096
RuO_2	2.18	806	1,455
CrO_3	2.02	1,608	2,297
MoO_3	1.75	1,117	1,521
V_2O_5	1.44	1,474	1,533
$LiFePO_4$	3.4	170	578
$LiMnPO_4$	4.1	171	701
$LiCoPO_4$	4.8	167	802
$LiNiPO_4$	5.1	167	852
Li_2FeSiO_4	3.3	328	1,082
Li_2MnSiO_4	4.0	333	1,332
Li_2CoSiO_4	4.3	325	1,397
Li_2NiSiO_4	4.7	326	1,530

theoretical specific capacity is 3,862 mAh g^{-1}. The electrochemical process is a three-phase boundary problem, and the reversible reduction/oxidation reaction of O_2 can be carried out using a porous carbon support loaded with an appropriate catalyst. Cells made of nanostructured transition metal oxide catalysts such as MnO_2, Co_3O_4, and Fe_3O_4 (127–129) and carbon nanostructures such as nanofibers (130) and graphene (131) have been assembled to obtain a reversible capacity of 1,000–2,000 mAh g^{-1}, although the initial capacity can be as high as 5,000 mAh g^{-1}. There are many hurdles to commercialization of Li-air technology. Safety issues owing to Li dendrite formation and catastrophic failure are of most concern. Irreversible side reactions and poor cycling stability, clogging of carbon support pores and catalyst deactivation, and large hysteresis in the charge/discharge cycles are technical issues that need to be overcome (126, 127, 132–134).

Another potential redox reaction for the cathode involves sulfur. The ring structure of S_8 can be reduced into chain-like polysulfide anions and eventually into Li_2S through multistage reactions to yield a theoretical capacity of 1,675 mAh g^{-1}. At present, known technical issues include dissolution of polysulfide anions into the organic electrolyte and deposition onto the anode, resulting in self-discharge of the Li-S battery at a rate as high as 8–15% per month (68, 83, 135). Flammability and toxicity of sulfur vapor are also of concern.

One of the most efficient ways to circumvent this is to fill functionalized channels of a mesoporous carbon framework with sulfur, which prevents the trapped sulfur from leaching out while providing sufficient access to Li ions and an intimate connection for electron transfer to the insulating sulfur (136–138). By impregnating molten sulfur into polyethylene glycol–functionalized

mesoporous carbon matrix, a nanostructured sulfur/carbon composite delivered a stable discharge capacity of 1,320 mAh g^{-1} at a current rate of 168 mA g^{-1} (133). Similarly, a sulfur/carbon composite fabricated by diffusing molten sulfur into microporous carbon spheres exhibited a capacity of 820 mAh g^{-1} at a current rate of 400 mA g^{-1} with excellent rate and cycling performance (139). Interestingly, further studies on graphene/sulfur composites demonstrated that graphene sheets were capable of stabilizing sulfur in the same manner by sandwiching it between the carbonaceous layers (140, 141). However, to achieve long-term reliability and thermal stability for practical implementation, modification of all components, that is, the anode, electrolyte, and cathode, particularly appropriate selection of the solid-state electrolyte, is highly desirable (83, 135).

Advancements in electrochemically active organic molecules, such as conducting polymers and redox polymers, have inspired further exploration of organic cathode materials with superior sustainability and degradability (142). A class of active organic molecules that can be prepared from natural sugars common in living systems has drawn considerable attention, and capacities of 200–300 mAh g^{-1} along with an operating voltage of 2–3 V have been achieved in $Li_xC_6O_6$ organic cathodes (143–145). These multifunctional biocompatible devices could find potential applications in wearable electronics and implantable components, although it is rather difficult to address their inherent disadvantages such as flammability, instability, low volumetric energy density, and high solubility in liquid electrolytes.

ELECTROLYTE

The electrolyte is one of the most important, and most often overlooked, components of a Li-ion battery. In addition to its primary function of shuttling Li ions between the two electrodes, reductive decomposition of the electrolyte is the main contributor to the formation of SEI. Because typical cell voltages for Li-ion batteries are beyond the voltage for decomposition of water and lithium is highly reactive to water, organic solvents are generally used for electrolyte solutions. Electrolytes consist of an organic solvent, typically a combination of ethylene carbonate, dimethyl carbonate, and diethyl carbonate, with a lithium salt, such as $LiPF_6$, $LiBF_4$, LiBOB [lithium bis(oxalato)borate], or $LiClO_4$. The ionic conductivity increases with temperature and is $\sim 10^{-2}$ S cm^{-1} at room temperature.

The next generation of high-energy and high-power batteries most likely will require a high cell voltage with extremely active anode and cathode materials that can operate over a large potential window. Protective surfaces on these highly reactive materials are critical for the safe operation of these new systems, and novel electrolyte materials will be essential. Toward this goal, a multitude of studies have been performed on redox shuttles and intelligent separators as well as ionic liquids and silicon-containing electrolytes.

Currently, cell overcharging is a serious problem that can lead to a reduction in reversible capacity and cycling life as well as create hazardous safety conditions including thermal runaway and even catastrophic failure of the battery. Reliable overcharge protection systems are a major obstacle to wide commercialization of many systems for high-voltage applications. A redox shuttle is an electrolyte additive that can be reversibly oxidized and reduced at a particular voltage to carry the excess current between the two electrodes. The redox shuttle essentially acts as a shunt whenever the cathode potential exceeds the particular oxidative potential of the shuttle molecule (146–148). For example, for a $LiFePO_4$ cathode that reaches a fully charged state at approximately 3.5 V, a shuttle molecule (S) with a redox potential slightly greater than 3.5 V (e.g., 3.7 V) can be used. During overcharge, the cell potential reaches the redox potential of the shuttle molecule, at which point the molecule is oxidized to S^+, and then diffuses to the anode to be reduced back to S, regenerating the shuttle molecule. To be practical, both the oxidized and reduced state of

the shuttle must be extremely stable throughout battery operation. Many molecules demonstrate reversible redox activity in the desired voltage ranges (149), but few exhibit the necessary stability. Additionally, one of the main issues in using redox shuttles is that they are efficient only when cell charging is limited to low rates.

One of the current shutdown methods in commercial Li-ion batteries uses a thermal transition in the separator material, which physically separates the two electrodes from making electrical contact. Common materials used for separators include polyethylene (PE), polypropylene (PP), and their laminates. When a cell overheats, a microporous plastic film that separates the anode and cathode electrodes melts and closes the pores, effectively stopping ion transport in the cell and shutting down the battery. The temperature at which this process occurs depends on the polymer; PE transitions at 135°C and PP at 165°C (150). This is an irreversible process; the battery cannot be reused after the shutdown. An interesting new area of research is in the development of novel intelligent separators that are able to reversibly shut down many times, thus preserving the utility of the battery without compromising safety or performance characteristics.

The present electrolyte system is optimized for graphitic anode and $LiCoO_2$ cathode materials. As new generations of anodes and cathodes are developed, they may require new electrolyte systems for optimal operation, including safety. New electrolyte systems include ionic liquids and the polyethylene oxide (PEO) system. We restrict our brief discussion to the PEO system as the solvent. This solvent system can be either in liquid form (low molecular weight or elevated operating temperature) and used in traditional liquid Li-ion batteries, or in the solid state (high molecular weight) for solid Li-polymer batteries.

PEO is a good Li ion conductor at elevated temperatures, but it suffers from poor ionic conductivity at room temperature ($\sim 10^{-7}$ S cm^{-1}) owing to its high degree of crystallinity. To overcome this limitation, one approach is to tether pendant oligo(ethylene oxide) chains to a polysiloxane backbone to improve its conductivity and physical properties. Polysiloxanes are ideal for this purpose because they exhibit high free volumes (151) and low glass transition temperatures owing to their highly flexible siloxane chains. These properties promote ion transport and can provide ion-hopping sites for the transfer of Li ions along the polymer backbone, whereas the oligo(ethylene oxide) moiety is able to complex the Li ions. Additionally, polysiloxanes are nontoxic, nonflammable, highly resistant to oxidation, and biocompatible. This approach is able to increase the ion conductivity of PEO-based electrolytes to as high as $\sim 10^{-4}$ S cm^{-1} at room temperature. To further increase the conductivity, the size of the polysiloxane backbone can be decreased to smaller oligosiloxane units by following the known inverse relationship between solvent viscosity and conductivity (152, 153). That is, the greater the solvent viscosity (or equivalently, the greater the molecular weight of the polymer), the lower the ionic conductivity will be. Indeed, when the oligosiloxane group is reduced to a single Si-O unit (silane group), the ionic conductivity can reach as high as $\sim 10^{-3}$ S cm^{-1} at room temperature (154), close to that of conventional electrolytes at room temperature.

CONCLUSION

Although the Li-ion battery is already a commercial product, its market potential increases exponentially with improved performance, particularly increased energy density. We discussed the requirements for the transportation industry and summarized research and development aiming at achieving these goals. There has been tremendous progress in improving the anode materials, but the cathode materials are faced with significantly more difficult challenges. Although this review covers the three major electrochemically active components of a battery, other inactive components are equally important for safety, easy packaging and recycling, heat management,

and other characteristics that are critical to overall battery pack performance. Many research and development opportunities await creative solutions with tremendous economic implications and environmental impact.

DISCLOSURE STATEMENT

H.H.K. receives funding from the U.S. Department of Energy to support work on battery electrode materials and is an author on U.S. Patent Application 13106210, "Graphene materials having randomly distributed two-dimensional structural defects," which was filed May 12, 2011.

ACKNOWLEDGMENTS

This review was written when the authors were supported by the U.S. Department of Energy, Basic Energy Sciences, grant DE-AC02-06CH11357 through the Center for Electrical Energy Storage, an Energy Frontier Research Center.

LITERATURE CITED

1. Int. Energy Agency. 2011. *Technology Roadmap: Electric and Plug-In Hybrid Electric Vehicles.* Paris: Int. Energy Agency. **http://www.iea.org/papers/2011/EV_PHEV_Roadmap.pdf**
2. Cairns EJ, Albertus P. 2010. Batteries for electric and hybrid-electric vehicles. *Annu. Rev. Chem. Biomol. Eng.* 1:299–320
3. Wagner FT, Lakshmanan B, Mathias MF. 2010. Electrochemistry and the future of the automobile. *J. Phys. Chem. Lett.* 1:2204–19
4. US Department of Energy, Energy Efficiency and Renewable Energy. 2011. *Fuel economy: where the energy goes.* **http://www.fueleconomy.gov/feg/atv.shtml**
5. US Department of Energy. 2011. Buying an energy-efficient electric motor. *Fact Sheet.* **http://www1.eere.energy.gov/industry/bestpractices/pdfs/mc-0382.pdf**
6. Winter M, Brodd RJ. 2004. What are batteries, fuel cells, and supercapacitors? *Chem. Rev.* 104:4245–69
7. Chan CK, Ruffo R, Hong SS, Cui Y. 2009. Surface chemistry and morphology of the solid electrolyte interphase on silicon nanowire lithium-ion battery anodes. *J. Power Sources* 189:1132–40
8. Chang ZR, Lv HJ, Tang HW, Li HJ, Yuan XZ, Wang HJ. 2009. Synthesis and characterization of high-density $LiFePO_4$/C composites as cathode materials for lithium-ion batteries. *Electrochim. Acta* 54:4595–99
9. Megahed S, Scrosati B. 1994. Lithium-ion rechargeable batteries. *J. Power Sources* 51:79–104
10. Qi Y, Harris SJ. 2010. In situ observation of strains during lithiation of a graphite electrode. *J. Electrochem. Soc.* 157:A741–47
11. Dey AN. 1971. Electrochemical alloying of lithium in organic electrolytes. *J. Electrochem. Soc.* 118:1547–49
12. Huggins RA. 1999. Lithium alloy negative electrodes. *J. Power Sources* 81:13–19
13. Winter M, Besenhard JO, Spahr ME, Novak P. 1998. Insertion electrode materials for rechargeable lithium batteries. *Adv. Mater.* 10:725–63
14. Larcher D, Beattie S, Morcrette M, Edstroem K, Jumas JC, Tarascon JM. 2007. Recent findings and prospects in the field of pure metals as negative electrodes for Li-ion batteries. *J. Mater. Chem.* 17:3759–72
15. Obrovac MN, Christensen L. 2004. Structural changes in silicon anodes during lithium insertion/extraction. *Electrochem. Solid State Lett.* 7:A93–96
16. Wen CJ, Huggins RA. 1981. Chemical diffusion in intermediate phases in the lithium-silicon system. *J. Solid State Chem.* 37:271–78
17. Nesper R, Vonschnering HG. 1987. $Li_{21}Si_5$, a Zintl phase as well as a Hume-Rothery phase. *J. Solid State Chem.* 70:48–57

18. Li J, Dahn JR. 2007. An in situ X-ray diffraction study of the reaction of Li with crystalline Si. *J. Electrochem. Soc.* 154:A156–61
19. Li H, Huang XJ, Chen LQ, Zhou GW, Zhang Z, et al. 2000. The crystal structural evolution of nano-Si anode caused by lithium insertion and extraction at room temperature. *Solid State Ionics* 135:181–91
20. Limthongkul P, Jang YI, Dudney NJ, Chiang YM. 2003. Electrochemically-driven solid-state amorphization in lithium-silicon alloys and implications for lithium storage. *Acta Mater.* 51:1103–13
21. Limthongkul P, Jang YI, Dudney NJ, Chiang YM. 2003. Electrochemically-driven solid-state amorphization in lithium-metal anodes. *J. Power Sources* 119:604–9
22. Obrovac MN, Krause LJ. 2007. Reversible cycling of crystalline silicon powder. *J. Electrochem. Soc.* 154:A103–8
23. Key B, Bhattacharyya R, Morcrette M, Seznec V, Tarascon JM, Grey CP. 2009. Real-time NMR investigations of structural changes in silicon electrodes for lithium-ion batteries. *J. Am. Chem. Soc.* 131:9239–49
24. Key B, Morcrette M, Tarascon JM, Grey CP. 2011. Pair distribution function analysis and solid state NMR studies of silicon electrodes for lithium ion batteries: understanding the (de)lithiation mechanisms. *J. Am. Chem. Soc.* 133:503–12
25. Chan CK, Peng HL, Liu G, McIlwrath K, Zhang XF, et al. 2008. High-performance lithium battery anodes using silicon nanowires. *Nat. Nanotechnol.* 3:31–35
26. Goldman JL, Long BR, Gewirth AA, Nuzzo RG. 2011. Strain anisotropies and self-limiting capacities in single-crystalline 3D silicon microstructures: models for high energy density lithium-ion battery anodes. *Adv. Funct. Mater.* 21:2412–22
27. Timmons A, Dahn JR. 2007. Isotropic volume expansion of particles of amorphous metallic alloys in composite negative electrodes for Li-ion batteries. *J. Electrochem. Soc.* 154:A444–48
28. Lee JK, Smith KB, Hayner CM, Kung HH. 2010. Silicon nanoparticles-graphene paper composites for Li ion battery anodes. *Chem. Commun.* 46:2025–27
29. Sandu I, Moreau P, Guyomard D, Brousse T, Roue L. 2007. Synthesis of nanosized Si particles via a mechanochemical solid-liquid reaction and application in Li-ion batteries. *Solid State Ionics* 178:1297–303
30. Zhang T, Zhang HP, Yang LC, Wang B, Wu YP, Takamura T. 2008. The structural evolution and lithiation behavior of vacuum-deposited Si film with high reversible capacity. *Electrochim. Acta* 53:5660–64
31. Maranchi JP, Hepp AF, Evans AG, Nuhfer NT, Kumta PN. 2006. Interfacial properties of the a-Si/Cu: active-inactive thin-film anode system for lithium-ion batteries. *J. Electrochem. Soc.* 153:A1246–53
32. Arie AA, Song JO, Lee JK. 2009. Structural and electrochemical properties of fullerene-coated silicon thin film as anode materials for lithium secondary batteries. *Mater. Chem. Phys.* 113:249–54
33. Kim WB, Ahn HJ, Kim YS, Sung YE, Seong TY. 2006. Formation and characterization of Cu-Si nanocomposite electrodes for rechargeable Li batteries. *J. Power Sources* 163:211–14
34. Wen ZY, Wang XY, Liu Y, Xu XG, Lin J. 2009. Preparation and characterization of a new nanosized silicon-nickel-graphite composite as anode material for lithium ion batteries. *J. Power Sources* 189:121–26
35. Liu WR, Wu NL, Shieh DT, Wu HC, Yang MH, et al. 2007. Synthesis and characterization of nanoporous NiSi-Si composite anode for lithium-ion batteries. *J. Electrochem. Soc.* 154:A97–102
36. Kim H, Han B, Choo J, Cho J. 2008. Three-dimensional porous silicon particles for use in high-performance lithium secondary batteries. *Angew. Chem. Int. Ed.* 47:10151–54
37. Cho J. 2010. Porous Si anode materials for lithium rechargeable batteries. *J. Mater. Chem.* 20:4009–14
38. Magasinski A, Dixon P, Hertzberg B, Kvit A, Ayala J, Yushin G. 2010. High-performance lithium-ion anodes using a hierarchical bottom-up approach. *Nat. Mater.* 9:353–58
39. Beattie SD, Larcher D, Morcrette M, Simon B, Tarascon JM. 2008. Si electrodes for Li-ion batteries—a new way to look at an old problem. *J. Electrochem. Soc.* 155:A158–63
40. Lu ZW, Zhang LQ, Liu XJ. 2010. Microstructure and electrochemical performance of Si-SiO_2-C composites as the negative material for Li-ion batteries. *J. Power Sources* 195:4304–7
41. Lee JH, Kim WJ, Kim JY, Lim SH, Lee SM. 2008. Spherical silicon/graphite/carbon composites as anode material for lithium-ion batteries. *J. Power Sources* 176:353–58
42. Xu WL, Flake JC. 2010. Composite silicon nanowire anodes for secondary lithium-ion cells. *J. Electrochem. Soc.* 157:A41–45

43. Lestriez B, Desaever S, Danet J, Moreau P, Plee D, Guyomard D. 2009. Hierarchical and resilient conductive network of bridged carbon nanotubes and nanofibers for high-energy Si negative electrodes. *Electrochem. Solid State Lett.* 12:A76–80
44. Hochgatterer NS, Schweiger MR, Koller S, Raimann PR, Wohrle T, et al. 2008. Silicon/graphite composite electrodes for high-capacity anodes: influence of binder chemistry on cycling stability. *Electrochem. Solid State Lett.* 11:A76–80
45. Bridel JS, Azais T, Morcrette M, Tarascon JM, Larcher D. 2010. Key parameters governing the reversibility of Si/carbon/CMC electrodes for Li-ion batteries. *Chem. Mater.* 22:1229–41
46. Takamura T, Ohara S, Uehara M, Suzuki J, Sekine K. 2004. A vacuum deposited Si film having a Li extraction capacity over 2000 mAh/g with a long cycle life. *J. Power Sources* 129:96–100
47. Idota Y, Kubota T, Matsufuji A, Maekawa Y, Miyasaka T. 1997. Tin-based amorphous oxide: a high-capacity lithium-ion-storage material. *Science* 276:1395–97
48. Yang J, Winter M, Besenhard JO. 1996. Small particle size multiphase Li-alloy anodes for lithium-ion-batteries. *Solid State Ionics* 90:281–87
49. Kepler KD, Vaughey JT, Thackeray MM. 1999. $Li_xCu_6Sn_5$ ($0 < x < 13$): an intermetallic insertion electrode for rechargeable lithium batteries. *Electrochem. Solid State Lett.* 2:307–9
50. Trahey L, Vaughey JT, Kung HH, Thackeray MM. 2009. High-capacity, microporous Cu_6Sn_5-Sn anodes for Li-ion batteries. *J. Electrochem. Soc.* 156:A385–89
51. Tang YF, Yang L, Qiu Z, Huang JS. 2009. Template-free synthesis of mesoporous spinel lithium titanate microspheres and their application in high-rate lithium ion batteries. *J. Mater. Chem.* 19:5980–84
52. Poizot P, Laruelle S, Grugeon S, Dupont L, Tarascon JM. 2000. Nano-sized transition-metal oxides as negative-electrode materials for lithium-ion batteries. *Nature* 407:496–99
53. Geim AK, Novoselov KS. 2007. The rise of graphene. *Nat. Mater.* 6:183–91
54. Novoselov KS, Geim AK, Morozov SV, Jiang D, Zhang Y, et al. 2004. Electric field effect in atomically thin carbon films. *Science* 306:666–69
55. Yoo E, Kim J, Hosono E, Zhou H, Kudo T, Honma I. 2008. Large reversible Li storage of graphene nanosheet families for use in rechargeable lithium ion batteries. *Nano Lett.* 8:2277–82
56. Magasinski A, Zdyrko B, Kovalenko I, Hertzberg B, Burtovyy R, et al. 2010. Toward efficient binders for Li-ion battery Si-based anodes: polyacrylic acid. *ACS Appl. Mater. Interfaces* 2:3004–10
57. Kovalenko I, Zdyrko B, Magasinski A, Hertzberg B, Milicev Z, et al. 2011. A major constituent of brown algae for use in high-capacity Li-ion batteries. *Science* 334:75–79
58. Zhang Z, Zhang L, Amine K. 2011. *Advanced electrolyte additives for PHEV/EV lithium-ion battery*. Presented at Veh. Technol. Program Annu. Merit Rev. Peer Eval. Meet., Washington, DC
59. Schweiger HG, Multerer M, Schweizer-Berberich M, Gores HJ. 2008. Optimization of cycling behavior of lithium ion cells at 60°C by additives for electrolytes based on lithium bis[1,2-oxalato(2-)-O,O′] borate. *Int. J. Electrochem. Sci.* 3:427–43
60. Lee JK, Kung MC, Trahey L, Missaghi MN, Kung HH. 2009. Nanocomposites derived from phenol-functionalized Si nanoparticles for high performance lithium ion battery anodes. *Chem. Mater.* 21:6–8
61. Zhang HG, Yu XD, Braun PV. 2011. Three-dimensional bicontinuous ultrafast-charge and -discharge bulk battery electrodes. *Nat. Nanotechnol.* 6:277–81
62. Park MH, Kim MG, Joo J, Kim K, Kim J, et al. 2009. Silicon nanotube battery anodes. *Nano Lett.* 9:3844–47
63. Zhao X, Hayner CM, Kung MC, Kung HH. 2011. In-plane vacancy-enabled high-power Si-graphene composite electrodes for lithium-ion batteries. *Adv. Energy Mater.* 1:1079–84
64. Whittingham MS. 2004. Lithium batteries and cathode materials. *Chem. Rev.* 104:4271–301
65. Wang Y, Cao GZ. 2008. Developments in nanostructured cathode materials for high-performance lithium-ion batteries. *Adv. Mater.* 20:2251–69
66. Thackeray MM, David WIF, Bruce PG, Goodenough JB. 1983. Lithium insertion into manganese spinels. *Mater. Res. Bull.* 18:461–72
67. Manthiram A, Murugan AV, Sarkar A, Muraliganth T. 2008. Nanostructured electrode materials for electrochemical energy storage and conversion. *Energy Environ. Sci.* 1:621–38
68. Goodenough JB, Kim Y. 2010. Challenges for rechargeable Li batteries. *Chem. Mater.* 22:587–603

69. Yuan LX, Wang ZH, Zhang WX, Hu XL, Chen JT, et al. 2011. Development and challenges of $LiFePO_4$ cathode material for lithium-ion batteries. *Energy Environ. Sci.* 4:269–84
70. Fisher CAJ, Prieto VMH, Islam MS. 2008. Lithium battery materials $LiMPO_4$ (M = Mn, Fe, Co, and Ni): insights into defect association, transport mechanisms, and doping behavior. *Chem. Mater.* 20:5907–15
71. Ammundsen B, Paulsen J. 2001. Novel lithium-ion cathode materials based on layered manganese oxides. *Adv. Mater.* 13:943–56
72. Thackeray MM, Kang SH, Johnson CS, Vaughey JT, Benedek R, Hackney SA. 2007. Li_2MnO_3-stabilized $LiMO_2$ (M = Mn, Ni, Co) electrodes for lithium-ion batteries. *J. Mater. Chem.* 17:3112–25
73. Nazri G-A, Pistoia G. 2009. *Lithium Batteries: Science and Technology*. New York: Springer
74. Ohzuku T, Kitagawa M, Hirai T. 1990. Electrochemistry of manganese-dioxide in lithium nonaqueous cell. III. X-ray diffractional study on the reduction of spinel-related manganese dioxide. *J. Electrochem. Soc.* 137:769–75
75. Tarascon JM, Wang E, Shokoohi FK, Mckinnon WR, Colson S. 1991. The spinel phase of $LiMn_2O_4$ as a cathode in secondary lithium cells. *J. Electrochem. Soc.* 138:2859–64
76. Kanevskii LS, Dubasova VS. 2005. Degradation of lithium-ion batteries and how to fight it: a review. *Russ. J. Electrochem.* 41:1–16
77. Song D, Ikuta H, Uchida T, Wakihara M. 1999. The spinel phases $LiAl_yMn_{2-y}O_4$ (y = 0, 1/12, 1/9, 1/6, 1/3) and $Li(Al,M)_{1/6}Mn_{11/6}O_4$ (M = Cr, Co) as the cathode for rechargeable lithium batteries. *Solid State Ionics* 117:151–56
78. Spahr ME, Novak P, Haas O, Nesper R. 1997. Cycling performance of novel lithium insertion electrode materials based on the Li-Ni-Mn-O system. *J. Power Sources* 68:629–33
79. Thackeray MM, Kang SH, Johnson CS, Vaughey JT, Hackney SA. 2006. Comments on the structural complexity of lithium-rich $Li_{1+x}M_{1-x}O_2$ electrodes (M = Mn, Ni, Co) for lithium batteries. *Electrochem. Commun.* 8:1531–38
80. Padhi AK, Nanjundaswamy KS, Goodenough JB. 1997. Phospho-olivines as positive-electrode materials for rechargeable lithium batteries. *J. Electrochem. Soc.* 144:1188–94
81. Manthiram A. 2009. Phospho-olivine cathodes for lithium-ion batteries. *Electrochem. Soc. Interface* 18(1):44–47
82. Padhi AK, Nanjundaswamy KS, Masquelier C, Okada S, Goodenough JB. 1997. Effect of structure on the Fe^{3+}/Fe^{2+} redox couple in iron phosphates. *J. Electrochem. Soc.* 144:1609–13
83. Scrosati B, Garche J. 2010. Lithium batteries: status, prospects and future. *J. Power Sources* 195:2419–30
84. Zhou H, Upreti S, Chernova NA, Hautier G, Ceder G, Whittingham MS. 2011. Iron and manganese pyrophosphates as cathodes for lithium-ion batteries. *Chem. Mater.* 23:293–300
85. Chen HL, Grey CP. 2008. Molten salt synthesis and high rate performance of the "desert-rose" form of $LiCoO_2$. *Adv. Mater.* 20:2206–10
86. Saravanan K, Reddy MV, Balaya P, Gong H, Chowdari BVR, Vittal JJ. 2009. Storage performance of $LiFePO_4$ nanoplates. *J. Mater. Chem.* 19:605–10
87. Balaya P. 2008. Size effects and nanostructured materials for energy applications. *Energy Environ. Sci.* 1:645–54
88. Morgan D, Van der Ven A, Ceder G. 2004. Li conductivity in Li_xMPO_4 (M = Mn, Fe, Co, Ni) olivine materials. *Electrochem. Solid State Lett.* 7:A30–32
89. Islam MS, Driscoll DJ, Fisher CAJ, Slater PR. 2005. Atomic-scale investigation of defects, dopants, and lithium transport in the $LiFePO_4$ olivine-type battery material. *Chem. Mater.* 17:5085–92
90. Wang YG, He P, Zhou HS. 2011. Olivine $LiFePO_4$: development and future. *Energy Environ. Sci.* 4:805–17
91. Lee HW, Muralidharan P, Ruffo R, Mari CM, Cui Y, Kim DK. 2010. Ultrathin spinel $LiMn_2O_4$ nanowires as high power cathode materials for Li-ion batteries. *Nano Lett.* 10:3852–56
92. Baxter J, Bian ZX, Chen G, Danielson D, Dresselhaus MS, et al. 2009. Nanoscale design to enable the revolution in renewable energy. *Energy Environ. Sci.* 2:559–88
93. Jiao F, Bao JL, Hill AH, Bruce PG. 2008. Synthesis of ordered mesoporous Li-Mn-O spinel as a positive electrode for rechargeable lithium batteries. *Angew. Chem. Int. Ed.* 47:9711–16

94. Jiao F, Bruce PG. 2007. Mesoporous crystalline β-MnO_2—a reversible positive electrode for rechargeable lithium batteries. *Adv. Mater.* 19:657–60
95. Okubo M, Mizuno Y, Yamada H, Kim J, Hosono E, et al. 2010. Fast Li-ion insertion into nanosized $LiMn_2O_4$ without domain boundaries. *ACS Nano* 4:741–52
96. Gibot P, Casas-Cabanas M, Laffont L, Levasseur S, Carlach P, et al. 2008. Room-temperature single-phase Li insertion/extraction in nanoscale Li_xFePO_4. *Nat. Mater.* 7:741–47
97. Owens BB, Passerini S, Smyrl WH. 1999. Lithium ion insertion in porous metal oxides. *Electrochim. Acta* 45:215–24
98. Lee K, Wang Y, Cao GH. 2005. Dependence of electrochemical properties of vanadium oxide films on their nano- and microstructures. *J. Phys. Chem. B* 109:16700–4
99. Chan CK, Peng HL, Twesten RD, Jarausch K, Zhang XF, Cui Y. 2007. Fast, completely reversible Li insertion in vanadium pentoxide nanoribbons. *Nano Lett.* 7:490–95
100. Li WY, Cheng FY, Tao ZL, Chen J. 2006. Vapor-transportation preparation and reversible lithium intercalation/deintercalation of α-MoO_3 microrods. *J. Phys. Chem. B* 110:119–24
101. Mai LQ, Hu B, Chen W, Qi YY, Lao CS, et al. 2007. Lithiated MoO_3 nanobelts with greatly improved performance for lithium batteries. *Adv. Mater.* 19:3712–16
102. Li CL, Gu L, Tsukimoto S, van Aken PA, Maier J. 2010. Low-temperature ionic-liquid-based synthesis of nanostructured iron-based fluoride cathodes for lithium batteries. *Adv. Mater.* 22:3650–54
103. Kim SW, Seo DH, Gwon H, Kim J, Kang K. 2010. Fabrication of FeF_3 nanoflowers on CNT branches and their application to high power lithium rechargeable batteries. *Adv. Mater.* 22:5260–64
104. Li T, Li L, Cao YL, Ai XP, Yang HX. 2010. Reversible three-electron redox behaviors of FeF_3 nanocrystals as high-capacity cathode-active materials for Li-ion batteries. *J. Phys. Chem. C* 114:3190–95
105. Arai H, Okada S, Sakurai Y, Yamaki J. 1997. Cathode performance and voltage estimation of metal trihalides. *J. Power Sources* 68:716–19
106. Wang YG, Wang YR, Hosono EJ, Wang KX, Zhou HS. 2008. The design of a $LiFePO_4$/carbon nanocomposite with a core-shell structure and its synthesis by an in situ polymerization restriction method. *Angew. Chem. Int. Ed.* 47:7461–65
107. Oh SM, Oh SW, Yoon CS, Scrosati B, Amine K, Sun YK. 2010. High-performance carbon-$LiMnPO_4$ nanocomposite cathode for lithium batteries. *Adv. Funct. Mater.* 20:3260–65
108. Sun XM, Li YD. 2004. Colloidal carbon spheres and their core/shell structures with noble-metal nanoparticles. *Angew. Chem. Int. Ed.* 43:597–601
109. Nien YH, Carey JR, Chen JS. 2009. Physical and electrochemical properties of $LiFePO_4$/C composite cathode prepared from various polymer-containing precursors. *J. Power Sources* 193:822–27
110. Wu XL, Jiang LY, Cao FF, Guo YG, Wan LJ. 2009. $LiFePO_4$ nanoparticles embedded in a nanoporous carbon matrix: superior cathode material for electrochemical energy-storage devices. *Adv. Mater.* 21:2710–14
111. Li CL, Gu L, Tong JW, Maier J. 2011. Carbon nanotube wiring of electrodes for high-rate lithium batteries using an imidazolium-based ionic liquid precursor as dispersant and binder: a case study on iron fluoride nanoparticles. *ACS Nano* 5:2930–38
112. Wilcox JD, Doeff MM, Marcinek M, Kostecki R. 2007. Factors influencing the quality of carbon coatings on $LiFePO_4$. *J. Electrochem. Soc.* 154:A389–95
113. Fu LJ, Liu H, Li C, Wu YP, Rahm E, et al. 2006. Surface modifications of electrode materials for lithium ion batteries. *Solid State Sciences* 8:113–28
114. Kim J, Noh M, Cho J, Kim H, Kim KB. 2005. Controlled nanoparticle metal phosphates (metal = Al, Fe, Ce, and Sr) coatings on $LiCoO_2$ cathode materials. *J. Electrochem. Soc.* 152:A1142–48
115. Sun YK, Lee YS, Yoshio M, Amine K. 2002. Synthesis and electrochemical properties of ZnO-coated $LiNi_{0.5}Mn_{1.5}O_4$ spinel as 5 V cathode material for lithium secondary batteries. *Electrochem. Solid State Lett.* 5:A99–102
116. Jung YS, Cavanagh AS, Riley LA, Kang SH, Dillon AC, et al. 2010. Ultrathin direct atomic layer deposition on composite electrodes for highly durable and safe Li-ion batteries. *Adv. Mater.* 22:2172–76
117. Zu CX, Li H. 2011. Thermodynamic analysis on energy densities of batteries. *Energy Environ. Sci.* 4:2614–24

118. Hautier G, Jain AK, Ong SP, Kang B, Moore C, et al. 2011. Phosphates as lithium-ion battery cathodes: an evaluation based on high-throughput ab initio calculations. *Chem. Mater.* 23:3495–508
119. Goodenough JB, Kim Y. 2011. Challenges for rechargeable batteries. *J. Power Sources* 196:6688–94
120. Li H, Balaya P, Maier J. 2004. Li-storage via heterogeneous reaction in selected binary metal fluorides and oxides. *J. Electrochem. Soc.* 151:A1878–85
121. Ohzuku T, Brodd RJ. 2007. An overview of positive-electrode materials for advanced lithium-ion batteries. *J. Power Sources* 174:449–56
122. Howard WF, Spotnitz RM. 2007. Theoretical evaluation of high-energy lithium metal phosphate cathode materials in Li-ion batteries. *J. Power Sources* 165:887–91
123. Amatucci GG, Pereira N. 2007. Fluoride based electrode materials for advanced energy storage devices. *J. Fluor. Chem.* 128:243–62
124. Abraham KM, Jiang Z. 1996. A polymer electrolyte-based rechargeable lithium/oxygen battery. *J. Electrochem. Soc.* 143:1–5
125. Lee KT, Lee JS, Kim ST, Cao R, Choi NS, et al. 2011. Metal-air batteries with high energy density: Li-air versus Zn-air. *Adv. Energy Mater.* 1:34–50
126. Ogasawara T, Debart A, Holzapfel M, Novak P, Bruce PG. 2006. Rechargeable Li_2O_2 electrode for lithium batteries. *J. Am. Chem. Soc.* 128:1390–93
127. Debart A, Paterson AJ, Bao J, Bruce PG. 2008. α-MnO_2 nanowires: a catalyst for the O_2 electrode in rechargeable lithium batteries. *Angew. Chem. Int. Ed.* 47:4521–24
128. Bruce PG. 2008. Energy storage beyond the horizon: rechargeable lithium batteries. *Solid State Ionics* 179:752–60
129. Debart A, Bao J, Armstrong G, Bruce PG. 2007. An O_2 cathode for rechargeable lithium batteries: the effect of a catalyst. *J. Power Sources* 174:1177–82
130. Mitchell RR, Gallant BM, Thompson CV, Shao-Horn Y. 2011. All-carbon-nanofiber electrodes for high-energy rechargeable Li-O_2 batteries. *Energy Environ. Sci.* 4:2952–58
131. Yoo E, Zhou HS. 2011. Li-air rechargeable battery based on metal-free graphene nanosheet catalysts. *ACS Nano* 5:3020–26
132. Read J. 2002. Characterization of the lithium/oxygen organic electrolyte battery. *J. Electrochem. Soc.* 149:A1190–95
133. Read J, Mutolo K, Ervin M, Behl W, Wolfenstine J, et al. 2003. Oxygen transport properties of organic electrolytes and performance of lithium/oxygen battery. *J. Electrochem. Soc.* 150:A1351–56
134. Xu W, Xiao J, Zhang J, Wang DY, Zhang JG. 2009. Optimization of nonaqueous electrolytes for primary lithium/air batteries operated in ambient environment. *J. Electrochem. Soc.* 156:A773–79
135. Hassoun J, Scrosati B. 2010. Moving to a solid-state configuration: a valid approach to making lithium-sulfur batteries viable for practical applications. *Adv. Mater.* 22:5198–201
136. Ji XL, Lee KT, Nazar LF. 2009. A highly ordered nanostructured carbon-sulphur cathode for lithium-sulphur batteries. *Nat. Mater.* 8:500–6
137. Yang Y, McDowell MT, Jackson A, Cha JJ, Hong SS, Cui Y. 2010. New nanostructured Li_2S/silicon rechargeable battery with high specific energy. *Nano Lett.* 10:1486–91
138. Lai C, Gao XP, Zhang B, Yan TY, Zhou Z. 2009. Synthesis and electrochemical performance of sulfur/highly porous carbon composites. *J. Phys. Chem. C* 113:4712–16
139. Zhang B, Qin X, Li GR, Gao XP. 2010. Enhancement of long stability of sulfur cathode by encapsulating sulfur into micropores of carbon spheres. *Energy Environ. Sci.* 3:1531–37
140. Cao YL, Li XL, Aksay IA, Lemmon J, Nie ZM, et al. 2011. Sandwich-type functionalized graphene sheet-sulfur nanocomposite for rechargeable lithium batteries. *Phys. Chem. Chem. Phys.* 13:7660–65
141. Wang HL, Yang Y, Liang YY, Robinson JT, Li YG, et al. 2011. Graphene-wrapped sulfur particles as a rechargeable lithium-sulfur battery cathode material with high capacity and cycling stability. *Nano Lett.* 11:2644–47
142. Armand M, Tarascon JM. 2008. Building better batteries. *Nature* 451:652–57
143. Nakahara K, Iwasa S, Satoh M, Morioka Y, Iriyama J, et al. 2002. Rechargeable batteries with organic radical cathodes. *Chem. Phys. Lett.* 359:351–54

144. Genorio B, Pirnat K, Cerc-Korosec R, Dominko R, Gaberscek M. 2010. Electroactive organic molecules immobilized onto solid nanoparticles as a cathode material for lithium-ion batteries. *Angew. Chem. Int. Ed.* 49:7222–24
145. Suga T, Konishi H, Nishide H. 2007. Photocrosslinked nitroxide polymer cathode-active materials for application in an organic-based paper battery. *Chem. Commun.* 2007:1730–32
146. Narayanan SR, Surampudi S, Attia AI, Bankston CP. 1991. Analysis of redox additive-based overcharge protection for rechargeable lithium batteries. *J. Electrochem. Soc.* 138:2224–29
147. Golovin MN, Wilkinson DP, Dudley JT, Holonko D, Woo S. 1992. Applications of metallocenes in rechargeable lithium batteries for overcharge protection. *J. Electrochem. Soc.* 139:5–10
148. Abraham KM. 1993. Directions in secondary lithium battery research-and-development. *Electrochim. Acta* 38:1233–48
149. Meites L, Zuman P. 1977–1983. *CRC Handbook Series in Organic Electrochemistry*, Vols. 1–6. Boca Raton, FL: CRC Press
150. Arora P, Zhang ZM. 2004. Battery separators. *Chem. Rev.* 104:4419–62
151. Zhang ZC, Sherlock D, West R, West R, Amine K, Lyons LJ. 2003. Cross-linked network polymer electrolytes based on a polysiloxane backbone with oligo(oxyethylene) side chains: synthesis and conductivity. *Macromolecules* 36:9176–80
152. Claes P, Simonis L, Glibert J. 1986. Properties of mixtures of zinc chloride and *N*-methylpyridinium chloride in the molten state—II. specific mass, electrical conductivity and viscosity. *Electrochim. Acta* 31:1525–30
153. Williams ME, Lyons LJ, Long JW, Murray RW. 1997. Transport and electron transfer dynamics in a polyether-tailed cobalt bipyridine molten salt: electrolyte effects. *J. Phys. Chem. B* 101:7584–91
154. Zhang LZ, Zhang ZC, Harring S, Straughan M, Butorac R, et al. 2008. Highly conductive trimethylsilyl oligo(ethylene oxide) electrolytes for energy storage applications. *J. Mater. Chem.* 18:3713–17

Annual Review of Chemical and Biomolecular Engineering

Volume 3, 2012

Contents

A Conversation with Haldor Topsøe
Haldor Topsøe and Manos Mavrikakis 1

Potential of Gold Nanoparticles for Oxidation in Fine Chemical Synthesis
Tamas Mallat and Alfons Baiker 11

Unraveling Reaction Pathways and Specifying Reaction Kinetics for Complex Systems
R. Vinu and Linda J. Broadbelt 29

Advances and New Directions in Crystallization Control
Zoltan K. Nagy and Richard D. Braatz 55

Nature Versus Nurture: Developing Enzymes That Function Under Extreme Conditions
Michael J. Liszka, Melinda E. Clark, Elizabeth Schneider, and Douglas S. Clark 77

Design of Nanomaterial Synthesis by Aerosol Processes
Beat Buesser and Sotiris E. Pratsinis 103

Single-Cell Analysis in Biotechnology, Systems Biology, and Biocatalysis
Frederik S.O. Fritzsch, Christian Dusny, Oliver Frick, and Andreas Schmid 129

Molecular Origins of Homogeneous Crystal Nucleation
Peng Yi and Gregory C. Rutledge 157

Green Chemistry, Biofuels, and Biorefinery
James H. Clark, Rafael Luque, and Avtar S. Matharu 183

Engineering Molecular Circuits Using Synthetic Biology in Mammalian Cells
Markus Wieland and Martin Fussenegger 209

Chemical Processing of Materials on Silicon: More Functionality, Smaller Features, and Larger Wafers
Nathan Marchack and Jane P. Chang 235

Engineering Aggregation-Resistant Antibodies
Joseph M. Perchiacca and Peter M. Tessier 263

Nanocrystals for Electronics
Matthew G. Panthani and Brian A. Korgel 287

Electrochemistry of Mixed Oxygen Ion and Electron Conducting Electrodes in Solid Electrolyte Cells
William C. Chueh and Sossina M. Haile 313

Experimental Methods for Phase Equilibria at High Pressures
Ralf Dohrn, José M.S. Fonseca, and Stephanie Peper 343

Density of States–Based Molecular Simulations
Sadanand Singh, Manan Chopra, and Juan J. de Pablo 369

Membrane Materials for Addressing Energy and Environmental Challenges
Enrico Drioli and Enrica Fontananova 395

Advances in Bioactive Hydrogels to Probe and Direct Cell Fate
Cole A. DeForest and Kristi S. Anseth 421

Materials for Rechargeable Lithium-Ion Batteries
Cary M. Hayner, Xin Zhao, and Harold H. Kung 445

Transport Phenomena in Chaotic Laminar Flows
Pavithra Sundararajan and Abraham D. Stroock 473

Sustainable Engineered Processes to Mitigate the Global Arsenic Crisis in Drinking Water: Challenges and Progress
Sudipta Sarkar, John E. Greenleaf, Anirban Gupta, Davin Uy, and Arup K. SenGupta 497

Complex Fluid-Fluid Interfaces: Rheology and Structure
Gerald G. Fuller and Jan Vermant 519

Atomically Dispersed Supported Metal Catalysts
Maria Flytzani-Stephanopoulos and Bruce C. Gates 521

Indexes

Cumulative Index of Contributing Authors, Volumes 1–3 575

Cumulative Index of Chapter Titles, Volumes 1–3 577

Errata

An online log of corrections to *Annual Review of Chemical and Biomolecular Engineering* articles may be found at http://chembioeng.annualreviews.org/errata.shtml